J. Fluid Mech. (1997), *vol.* 344, *pp.* 181–212. Printed in the United Kingdom

© 1997 Cambridge University Press

The initial value problem for Kelvin vortex waves

By STEVE ARENDT[1]†, DAVID C. FRITTS[1]† AND ØYVIND ANDREASSEN[2]

[1]Laboratory for Atmospheric and Space Physics, University of Colorado, Boulder, CO 80309-0392, USA

[2]Forsvarets Forskningsinstitutt, Kjeller, Norway

(Received 6 February 1996 and in revised form 14 March 1997)

We present a formal solution to the initial value problem for small perturbations of a straight vortex tube with constant vorticity, and show that any initial perturbation to such a tube evolves exclusively as a collection of Kelvin vortex waves. We then study in detail the evolution of the following particular initial states of the vortex tube: (i) an axisymmetric pinch in the radius of the tube, (ii) a deflection in the location of the tube, and (iii) a flattening of the tube's cross-secton. All of these initial states are localized in the direction along the tube by weighting them with a Gaussian function. In each case, the initial perturbation is decomposed into packets of Kelvin vortex waves which then propagate outward along the vortex tube. We discuss the physical mechanisms responsible for the propagation of the wave packets, and study the consequences of wave dispersion for the solution.

1. Introduction

Lord Kelvin (1880) was the first to note that a straight vortex tube of uniform vorticity and circular cross-section supports stable wave modes which propagate along the axis of the vortex tube. The modes are characterized by an azimuthal wavenumber m describing the azimuthal structure of the mode and a radial number n describing the radial structure of the mode (see Saffman 1992 for an introduction). A considerable amount of subsequent theoretical work has focused on waves for more general vortex core structures and waves which are not infinitesimal in amplitude (Hasimoto 1972; Moore & Saffman 1972; Leibovich & Ma 1983; Leibovich, Brown & Patel 1986). Several striking experimental studies (Hopfinger, Browand & Gagne 1982; Maxworthy, Hopfinger & Redekopp 1985) have shown the presence of waves on laboratory vortex tubes. Although Kelvin wave modes are stable in themselves, they are made unstable by the imposition of certain external flows. A well-known example is the long-wavelength Crow instability of a pair of counter-rotating vortices (Crow 1971). Here the external flow due to one tube destabilizes $m = 1$ Kelvin waves on the other tube. This may be considered as a special case of an external straining field destabilizing Kelvin waves (Moore & Saffman 1975; Tsai & Widnall 1976). The presence of an axial flow along the vortex tube has also been shown to destabilize wave modes on vortex tubes (Lessen, Singh & Paillet 1974; Mayer & Powell 1992).

† Present address: Colorado Research Associates/NWRA, 3380 Mitchell Lane, Boulder, CO 80301, USA.

https://doi.org/10.1017/S0022112097005958 Published online by Cambridge University Press

The excitation of wave modes has received much recent attention. Melander & Hussain (1994) have used a numerical simulation to study the evolution of axisymmetric core perturbations of a vortex tube. In their work, the core size initially varies periodically in the axial direction, and, as time progresses, the core variations propagate in a wave-like fashion. Melander & Hussain show that the propagation occurs because the core size variations of the vortex tube lead to an axial differential rotation and a consequent twisting of the vortex lines. The twisted vortex lines induce a meridional flow which then feeds back to change the core size. At later times, the waves form a low-enstrophy bubble in the centre of the vortex tube's core, and then die out due to viscosity. Further results discuss the importance of these waves in a plane mixing layer (Schoppa, Hussain & Metcalfe 1995) and in the interaction of a vortex with surrounding turbulence (Melander & Hussain 1993). Finally, we mention the work of Verzicco, Jiménez & Orlandi (1995) who study a vortex tube in an external axial straining. They find that the core dynamics of the tube opposes the straining so that the vortex tube reaches a steady state even when the strain is compressional.

In two companion papers (Andreassen *et al.* 1997; Fritts, Arendt & Andreassen 1997), we describe a numerical simulation of a breaking gravity wave and point out the prominent role that vortex waves, or twist waves†, have in the evolution of the flow. Briefly, the breaking gravity wave undergoes a series of instabilities which act to concentrate the vorticity of the flow into a collection of intertwined vortex loops. These vortex loops then suffer fragmentation and unravelling associated with $m = 0$ and $m = 2$ twist waves, where m refers to the azimuthal wavenumber of the wave around the tube. There is also evidence for $m = 1$ waves although these do not appear to influence the overall flow evolution as strongly as do the $m = 0$ and $m = 2$ waves.

Motivated by the importance of twist waves in the breaking gravity wave and by their possible importance in other turbulent flow evolutions (e.g. Cadot, Douady & Couder 1995), we present here analytic calculations of the evolution of a perturbed vortex tube. We begin with a solution to the initial value problem for small perturbations of a straight vortex tube with constant vorticity, and show that any initial perturbation to such a tube evolves exclusively as a collection of Kelvin waves. The continuous spectrum of modes found to be important in other situations (Case 1960) is not present in our case; only the discrete modes occur. We go on to study the evolution of the following initial states: (i) an axisymmetric pinch in the radius of the tube, (ii) a deflection in the location of the tube, and (iii) a flattening of the tube's cross-secton; these are examples of $m = 0$, $m = 1$ and $m = 2$ Kelvin waves, respectively. In each case, we discuss the physical mechanisms underlying the propagation of the resulting Kelvin wave packets. In particular, we find that the propagation of $m = 0$ Kelvin waves is due to the twisting of vortex lines and the subsequent induced meridional flow, i.e. the same mechanism as was found by Melander & Hussain (1994) for their core dynamics simulations. This leads us to conclude that the core dynamics observed by Melander & Hussain are the nonlinear analogue of Kelvin wave packets, a point we discuss in § 3.

The present paper is organized as follows. The solution of the initial value problem is developed in § 2. The later sections discuss particular examples using this formalism. These examples are organized by azimuthal wavenumber m, with § 3, § 4 and § 5 dealing with $m = 0$, $m = 1$, and $m = 2$, respectively. Section 6 summarizes the results and discusses their relation to the gravity wave simulations mentioned earlier. Three Appendices contain mathematical material necessary for the derivations.

† We will refer to a wave on a vortex tube as a twist wave because the physics of the wave's propagation depends crucially on the twist (ω_ϕ) of the vortex lines. Twist waves on a straight vortex tube of constant vorticity will be called Kelvin vortex waves or Kelvin waves.

https://doi.org/10.1017/S0022112097005958 Published online by Cambridge University Press

2. Solution of the initial value problem

In this section we solve the initial value problem for the time evolution of linearized perturbations on a straight vortex tube of constant vorticity. For the purposes of this paper, we are interested in the self-dynamics of the tube and not in the interaction of the tube with any surrounding vorticity; we thus limit our consideration to initial conditions corresponding to perturbations of the straight tube with irrotational (potential) flow outside.

We begin with the inviscid Euler equation

$$\frac{\partial \boldsymbol{u}}{\partial t} + (\boldsymbol{u}\cdot\nabla)\boldsymbol{u} = -\nabla\left(\frac{P}{\rho}\right) \tag{2.1}$$

and the incompressible continuity equation

$$\nabla\cdot\boldsymbol{u} = 0. \tag{2.2}$$

We define cylindrical coordinates (r, ϕ, z) and consider small perturbations about a straight vortex tube, taking the unperturbed vortex tube to have constant vorticity $\boldsymbol{\omega} = 2\Omega\hat{\boldsymbol{z}}$ and to have a circular cross-section of radius a. We linearize (2.1) and (2.2) about this state and take the perturbations to have a ϕ dependence of the form $\exp(\mathrm{i}m\phi)$. There is no loss of generality in this, as a general dependence on ϕ can be handled by a Fourier series in ϕ. Finally, we employ a Fourier transform in z. To avoid excessively complicated notation, we will denote a function and its Fourier transform by the same term, leaving it to the context to distinguish the two:

$$\boldsymbol{u}(r,\phi,k,t) = \int_{-\infty}^{\infty} \boldsymbol{u}(r,\phi,z,t)\mathrm{e}^{\mathrm{i}kz}\mathrm{d}z, \tag{2.3}$$

$$\boldsymbol{u}(r,\phi,z,t) = \frac{1}{2\pi}\int_{-\infty}^{\infty} \boldsymbol{u}(r,\phi,k,t)\mathrm{e}^{-\mathrm{i}kz}\mathrm{d}k. \tag{2.4}$$

Beginning with the flow inside the vortex tube, the components of the linearized Euler equation can be written as

$$\mathrm{D}u_z^i = \mathrm{i}k\frac{P}{\rho}, \tag{2.5}$$

$$\mathrm{D}u_r^i - 2\Omega u_\phi^i = -\frac{\partial}{\partial r}\frac{P}{\rho}, \tag{2.6}$$

$$\mathrm{D}u_\phi^i + 2\Omega u_r^i = -\frac{\mathrm{i}m}{r}\frac{P}{\rho}, \tag{2.7}$$

where the superscript i denotes the solutions inside the vortex tube (i.e. inside the vortex tube's perturbed boundary $r = a + \delta a$), and where the operator D is given by

$$\mathrm{D} = \left(\frac{\partial}{\partial t} + \mathrm{i}m\Omega\right). \tag{2.8}$$

To complete the set of equations, the continuity equation is

$$\frac{1}{r}\frac{\partial(ru_r^i)}{\partial r} + \frac{\mathrm{i}m}{r}u_\phi^i - \mathrm{i}ku_z^i = 0. \tag{2.9}$$

We now find a single equation for u_z^i from (2.5)–(2.9); u_z turns out to be the most convenient quantity with which to carry out the solution. Equations (2.5)–(2.7) can

https://doi.org/10.1017/S0022112097005958 Published online by Cambridge University Press

be manipulated to yield

$$(\mathrm{D}^2 + 4\Omega^2)u_r^i = -\frac{1}{\mathrm{i}k}\frac{\partial}{\partial r}(\mathrm{D}^2 u_z^i) - \frac{2\Omega m}{kr}\mathrm{D}u_z^i, \tag{2.10}$$

and

$$(\mathrm{D}^2 + 4\Omega^2)u_\phi^i = \frac{2\Omega}{\mathrm{i}k}\frac{\partial}{\partial r}(\mathrm{D}u_z^i) - \frac{m}{kr}\mathrm{D}^2 u_z^i. \tag{2.11}$$

Operating on the continuity equation (2.9) with $(\mathrm{D}^2+4\Omega^2)$ and using (2.10) and (2.11) we find

$$\mathrm{D}^2\left[\frac{\partial^2}{\partial r^2} + \frac{1}{r}\frac{\partial}{\partial r} - \frac{m^2}{r^2} - k^2\right]u_z^i - 4\Omega^2 k^2 u_z^i = 0. \tag{2.12}$$

This, then, is the equation to be solved for u_z^i as a function of t and r inside the vortex tube.

The equations for the external fields may be found by recalling that our initial condition has $\boldsymbol{\omega} = 0$ outside the vortex tube. Straightforward manipulation of $\nabla\cdot\boldsymbol{u}^o = 0$ and $\nabla \times \boldsymbol{u}^o = 0$ then yields

$$\left[\frac{\partial^2}{\partial r^2} + \frac{1}{r}\frac{\partial}{\partial r} - \frac{m^2}{r^2} - k^2\right]u_z^o = 0, \tag{2.13}$$

$$u_r^o = -\frac{1}{\mathrm{i}k}\frac{\partial u_z^o}{\partial r}, \tag{2.14}$$

$$u_\phi^o = -\frac{m}{kr}u_z^o, \tag{2.15}$$

where the superscript o denotes the solutions outside the vortex tube. Note that (2.13)–(2.15) contain no time derivatives.

The solution of (2.12) and (2.13) is completed by enforcing the continuity of u_z and u_r at the boundary of the vortex given by $r = a + \delta a$. To the correct order of perturbed quantities, this is the same as enforcing the continuity of u_z and u_r at $r = a$. The $\hat{\boldsymbol{\phi}}$-directed velocity perturbation u_ϕ is not continuous at $r = a$, although the total $\hat{\boldsymbol{\phi}}$-directed velocity is; this will be discussed later.†

Before proceeding, we digress to point out that if one seeks solutions of (2.12) and (2.13) that are harmonic in time and have a single wavenumber k, one recovers Kelvin vortex waves:

$$u_z^i(r,\phi,z) = C\frac{J_m(k\xi_n r)}{J_m(k\xi_n a)}\mathrm{e}^{\mathrm{i}(m\phi+\omega_n t-kz)}, \tag{2.16}$$

$$u_z^o(r,\phi,z) = C\frac{K_m(kr)}{K_m(ka)}\mathrm{e}^{\mathrm{i}(m\phi+\omega_n t-kz)}, \tag{2.17}$$

where C is a constant amplitude, and where the quantity ξ_n is given by

$$\xi_n^2 = \frac{4\Omega^2}{(\omega_n + m\Omega)^2} - 1. \tag{2.18}$$

The continuity of u_z at $r = a$ has already been accounted for in the construction of (2.16) and (2.17). Determining u_r^i and u_r^o from (2.10) and (2.14) and enforcing their

† Other boundary conditions that are sometimes used are the continuity of the total pressure and the condition that the vortex boundary moves with the flow. Both of these boundary conditions are satisfied implicitly by our condition that the velocity components be continuous.

https://doi.org/10.1017/S0022112097005958 Published online by Cambridge University Press

continuity at $r = a$ gives the eigenvalue relation

$$\frac{J'_m(k\xi_n a)}{k\xi_n a J_m(k\xi_n a)} + \frac{2m\Omega}{(k\xi_n a)^2(\omega_n + m\Omega)} + \frac{K'_m(ka)}{kaK_m(ka)} = 0. \tag{2.19}$$

Equation (2.19) may be thought of as an equation to be solved for ξ_n; ξ_n in turn gives ω_n via (2.18). The transcendental equation (2.19) has an infinite number of solutions for a given m. We denote this sequence by a radial number n so that the nth eigenvalue is ξ_n. The ξ_n increase in magnitude with increasing n, so that the wave modes have increasing radial structure with increasing n due to the oscillatory nature of the Bessel function $J_m(k\xi_n r)$. There is an interesting degeneracy hidden in the eigenvalue relation related to the multiple-valued nature of ω_n. Specifically, ω_n is given by

$$\omega_n + m\Omega = \pm 2\Omega/(\xi_n^2 + 1)^{1/2} = b2\Omega/(\xi_n^2 + 1)^{1/2}, \tag{2.20}$$

where $b = \pm 1$. Using this to rewrite (2.19), we find

$$\frac{J'_m(k\xi_n a)}{k\xi_n a J_m(k\xi_n a)} + \frac{bm(\xi_n^2 + 1)^{1/2}}{(k\xi_n a)^2} + \frac{K'_m(ka)}{kaK_m(ka)} = 0. \tag{2.21}$$

Clearly, $b = +1$ gives different ξ_n (and hence ω_n) than $b = -1$. One can show (Saffman 1992) that the $b = +1$ solutions are retrograde, i.e. their angular propagation in a reference frame moving with the unperturbed flow rotation, Ω, is in the direction opposite to that of the unperturbed flow rotation. Similarly, the $b = -1$ solutions are cograde so that their angular propagation in a reference frame moving with the unperturbed flow rotation, Ω, is in the same direction as the unperturbed flow rotation. As can be seen from (2.21), this degeneracy only exists for the $m \neq 0$ case. One finds that all the ω_n are real for both $b = \pm 1$ and for all m, so that all the wave modes are stable. The reader is referred to Saffman (1992) for further details.

Now, we are interested in a complete solution of the initial value problem for (2.12) and (2.13). Having the individual wave modes, one might be tempted to write a general solution as a superposition of modes, but this is typically only valid if the governing equation can be written in Sturm–Liouville form. In that case, properties of the set of wave modes such as completeness and orthogonality have been proven in general. In our case only the $m = 0$ case can be written in Sturm–Liouville form. Thus, we are forced to turn to more general methods, in particular the use of the Laplace transform (see e.g. Case 1960). When all is done, however, we will find that the solution can be written as a superposition of wave modes.

We proceed, then, with the solution using the Laplace transform; a tilde will denote transformed quantities

$$\tilde{f}(s) = \int_0^\infty \mathrm{e}^{-st} f(t)\mathrm{d}t. \tag{2.22}$$

Concentrating first on the fields inside the vortex tube, we transform equation (2.12), and find

$$\left[\frac{\partial^2}{\partial r^2} + \frac{1}{r}\frac{\partial}{\partial r} - \frac{m^2}{r^2} - k^2\left(1 + \frac{4\Omega^2}{(s + \mathrm{i}m\Omega)^2}\right)\right]\tilde{u}_z^i = F(0), \tag{2.23}$$

with

$$F(0) = \frac{1}{(s + \mathrm{i}m\Omega)^2}\left[\frac{\partial^2}{\partial r^2} + \frac{1}{r}\frac{\partial}{\partial r} - \frac{m^2}{r^2} - k^2\right]\frac{\partial \tilde{u}_z^i}{\partial t}(0) + \frac{(s + 2\mathrm{i}m\Omega)}{(s + \mathrm{i}m\Omega)^2}\left[\frac{\partial^2}{\partial r^2} + \frac{1}{r}\frac{\partial}{\partial r} - \frac{m^2}{r^2} - k^2\right]\tilde{u}_z^i(0), \tag{2.24}$$

https://doi.org/10.1017/S0022112097005958 Published online by Cambridge University Press

where the (0) denotes the $t = 0$ initial condition. Appendix A contains a simplified expression for $F(0)$ in terms of the initial vorticity distribution only. We will also need an expression for $\tilde{u}_r^i$ to apply the boundary conditions. Transforming (2.10) gives

$$\tilde{u}_r^i = -\frac{1}{\mathrm{i}k}\frac{1}{4\Omega^2 + (s + \mathrm{i}m\Omega)^2}\left[(s + \mathrm{i}m\Omega)^2\frac{\partial \tilde{u}_z^i}{\partial r} + (s + \mathrm{i}m\Omega)\frac{\mathrm{i}m2\Omega}{r}\tilde{u}_z^i\right] + G(0), \tag{2.25}$$

where

$$G(0) = \frac{1}{\mathrm{i}k}\frac{1}{4\Omega^2 + (s + \mathrm{i}m\Omega)^2}\left[\frac{\partial}{\partial r}\frac{\partial \tilde{u}_z^i}{\partial t}(0) + (s + 2\mathrm{i}m\Omega)\frac{\partial \tilde{u}_z^i(0)}{\partial r} + \frac{\mathrm{i}m2\Omega}{r}\tilde{u}_z^i(0)\right]$$
$$+\frac{1}{4\Omega^2 + (s + \mathrm{i}m\Omega)^2}\left[\frac{\partial \tilde{u}_r^i}{\partial t}(0) + (s + 2\mathrm{i}m\Omega)\tilde{u}_r^i(0)\right]. \tag{2.26}$$

Again, Appendix A contains a simplified expression for $G(0)$ in terms of the initial vorticity distribution only.

The equations for the flow external to the vortex tube follow from (2.13) and (2.14):

$$\left[\frac{\partial^2}{\partial r^2} + \frac{1}{r}\frac{\partial}{\partial r} - \frac{m^2}{r^2} - k^2\right]\tilde{u}_z^o = 0, \tag{2.27}$$

$$\tilde{u}_r^o = -\frac{1}{\mathrm{i}k}\frac{\partial \tilde{u}_z^o}{\partial r}. \tag{2.28}$$

The next step is to solve (2.23) and (2.27) for $\tilde{u}_z$ inside and outside the vortex tube. Noting that (2.23) is a form of Bessel's equation, we find

$$\tilde{u}_z^i(r, \phi, k) = AJ_m(k\xi r)\mathrm{e}^{\mathrm{i}m\phi} + g(r)\mathrm{e}^{\mathrm{i}m\phi}. \tag{2.29}$$

The function $g(r)$ is the solution due to the forcing term $F(0)$ on the right-hand side of (2.23)

$$g(r) = Y_m(k\xi r)\int^r F(0)J_m(k\xi r')\frac{\pi r'}{2}\mathrm{d}r' - J_m(k\xi r)\int^r F(0)Y_m(k\xi r')\frac{\pi r'}{2}\mathrm{d}r', \tag{2.30}$$

where we have used the fact that the Wronskian of the Bessel functions is given by $W(J_m(k\xi r'), Y_m(k\xi r')) = 2/(\pi k\xi r')$, and where ξ is defined by

$$\xi^2 = -\frac{4\Omega^2}{(s + \mathrm{i}m\Omega)^2} - 1. \tag{2.31}$$

This definition of ξ is consistent with the previous definition in (2.18) with $s = \mathrm{i}\omega$. From (2.27), the $\hat{\boldsymbol{z}}$-directed velocity outside the tube is simply

$$\tilde{u}_z^o(r, \phi, k) = BK_m(kr)\mathrm{e}^{\mathrm{i}m\phi}. \tag{2.32}$$

The constants A and B in (2.29) and (2.32) are undetermined coefficients to be obtained from the boundary conditions.

To apply the boundary conditions we require the radial velocity inside and outside the tube; these are found from (2.25) and (2.28) to be

$$\tilde{u}_r^i(r, \phi, k) = \frac{A}{\mathrm{i}\xi}\left[J_m'(k\xi r) + \frac{\mathrm{i}m2\Omega}{s + \mathrm{i}m\Omega}\frac{J_m(k\xi r)}{k\xi r}\right]\mathrm{e}^{\mathrm{i}m\phi}$$
$$+\frac{1}{\mathrm{i}k\xi^2}\left[g'(r) + \frac{\mathrm{i}m2\Omega}{s + \mathrm{i}m\Omega}\frac{g(r)}{r}\right]\mathrm{e}^{\mathrm{i}m\phi} + G(0)\mathrm{e}^{\mathrm{i}m\phi}, \tag{2.33}$$

$$\tilde{u}_r^o(r, \phi, k) = \mathrm{i}BK_m'(kr)\mathrm{e}^{\mathrm{i}m\phi}, \tag{2.34}$$

https://doi.org/10.1017/S0022112097005958 Published online by Cambridge University Press

where the primes on the Bessel functions denote derivatives with respect to their arguments.

The boundary conditions are the continuity of $\tilde{u}_z$ and $\tilde{u}_r$ at $r = a$. Enforcing these, we obtain the constants A and B:

$$A = \frac{1}{J_m(k\xi a)} \frac{-g(a)\dfrac{K'_m(ka)}{kaK_m(ka)} - \dfrac{1}{(k\xi a)^2}\left(ag'(a) + \dfrac{2\mathrm{i}m\Omega}{s+\mathrm{i}m\Omega}g(a)\right) - \dfrac{\mathrm{i}G(0)|_{r=a}}{ka}}{\dfrac{J'_m(k\xi a)}{k\xi aJ_m(k\xi a)} + \dfrac{2\mathrm{i}m\Omega}{(k\xi a)^2(s+\mathrm{i}m\Omega)} + \dfrac{K'_m(ka)}{kaK_m(ka)}}, \tag{2.35}$$

$$B = \frac{1}{K_m(ka)} \frac{\dfrac{J'_m(k\xi a)}{k\xi aJ_m(k\xi a)}g(a) - a\dfrac{g'(a)}{(k\xi a)^2} - \dfrac{\mathrm{i}G(0)|_{r=a}}{ka}}{\dfrac{J'_m(k\xi a)}{k\xi aJ_m(k\xi a)} + \dfrac{2\mathrm{i}m\Omega}{(k\xi a)^2(s+\mathrm{i}m\Omega)} + \dfrac{K'_m(ka)}{kaK_m(ka)}}. \tag{2.36}$$

It remains to invert the Laplace transform. Now, in Appendix B, we show that the Laplace transform can be inverted using the Cauchy residue theorem, wherein the inverse transform is found to be equal to the sum of the residues at the poles of the integrand. In our case, the poles lie at the Kelvin wave mode eigenvalues, a fact which can be seen by comparing the denominator of A and B given by (2.35) and (2.36) to the eigenvalue relation given in (2.19).

To obtain the residues at these poles, we expand the denominator of (2.35) and (2.36) around a solution of (2.21). To first order in $(s - s_n)$, the denominator becomes

$$\frac{(\xi_n^2+1)^{3/2}(s-s_n)}{2\Omega b\mathrm{i}\xi_n^2}\left[1 - \frac{m^2}{(k\xi_n a)^2} + 2\frac{J'_m(k\xi_n a)}{k\xi_n aJ_m(k\xi_n a)} + \left(\frac{J'_m(k\xi_n a)}{J_m(k\xi_n a)}\right)^2 + \frac{bm(\xi_n^2+2)}{(k\xi_n a)^2(\xi_n^2+1)^{1/2}}\right], \tag{2.37}$$

where ξ_n is the nth solution to the transcendental equation (2.21), and where s_n is given by (2.20) with $s_n = \mathrm{i}\omega_n$. As before, $b = \pm 1$ with $b = +1$ corresponding to retrograde waves and $b = -1$ corresponding to cograde waves.

Using (2.37) and the Cauchy residue theorem, we transform (2.29) and (2.32) to the time domain to find

$$u_z^i(r,\phi,k) = \sum_{b=\pm1}\sum_{n=1}^{\infty} \frac{J_m(k\xi_n r)}{J_m(k\xi_n a)} bC_n^b \mathrm{e}^{\mathrm{i}m\phi + s_n t}, \tag{2.38}$$

$$u_z^o(r,\phi,k) = \sum_{b=\pm1}\sum_{n=1}^{\infty} \frac{K_m(kr)}{K_m(ka)} bC_n^b \mathrm{e}^{\mathrm{i}m\phi + s_n t}, \tag{2.39}$$

where

$$C_n^b = \frac{2\Omega\mathrm{i}\xi_n^2}{(\xi_n^2+1)^{3/2}}\left[\frac{J'_m(k\xi_n a)}{k\xi_n aJ_m(k\xi_n a)}g(a) - \frac{ag'(a)}{(k\xi_n a)^2} - \frac{\mathrm{i}G(0)|_{r=a}}{ka}\right] \Bigg/ \left[1 - \frac{m^2}{(k\xi_n a)^2} + \frac{2J'_m(k\xi_n a)}{k\xi_n aJ_m(k\xi_n a)} + \left(\frac{J'_m(k\xi_n a)}{J_m(k\xi_n a)}\right)^2 + \frac{bm(\xi_n^2+2)}{(k\xi_n a)^2(\xi_n^2+1)^{1/2}}\right]. \tag{2.40}$$

We have used the dispersion relation (2.21) in the simplification of C_n^b. The functions

https://doi.org/10.1017/S0022112097005958 Published online by Cambridge University Press

$g(r)$, $F(0)$, and $G(0)$ are given by (2.30), (A 7) and (A 10), respectively. As a final step, we invert the Fourier transform to obtain

$$u_z^i(r,\phi,z) = \frac{1}{2\pi}\int_{-\infty}^{\infty}\sum_{b=\pm1}\sum_{n=1}^{\infty}\frac{J_m(k\xi_n r)}{J_m(k\xi_n a)}bC_n^b e^{im\phi+s_n t}e^{-ikz}dk, \tag{2.41}$$

$$u_z^o(r,\phi,z) = \frac{1}{2\pi}\int_{-\infty}^{\infty}\sum_{b=\pm1}\sum_{n=1}^{\infty}\frac{K_m(kr)}{K_m(ka)}bC_n^b e^{im\phi+s_n t}e^{-ikz}dk. \tag{2.42}$$

Equations (2.41) and (2.42) for u_z^i and u_z^o complete the formal solution to the initial value problem. The remaining velocity components u_r and u_ϕ may be found from (2.10), (2.11), (2.14), and (2.15), while the vorticity components are found from (C 3) in Appendix C.

Equations (2.41) and (2.42) yield the important result that any small perturbations to a straight vortex tube with constant vorticity are decomposed entirely into Kelvin vortex waves. It is interesting that our results do not contain a continuous spectrum of eigenmodes (Case 1960); only the discrete spectrum is present. This is possibly due to our choice of an unvarying vorticity within the vortex tube. The singularity $1/(\omega + m\Omega(r))$ which causes the continuous spectrum (see e.g. Briggs, Daugherty & Levy 1970) becomes $1/(\omega + m\Omega)$ ($1/D$ in our equation (2.12)) with Ω constant, and is only capable of contributing a discrete frequency. This discrete frequency, $\omega = -m\Omega$, is not to be confused with the discrete frequencies due to true three-dimensional wave modes; rather, it is the discrete version of the continuous spectrum. However, the frequency $\omega = -m\Omega$ is not present in the final three-dimensional solution (see Appendix B and note that the point $\omega = -m\Omega$ is the point at which the integrand is not analytic).

On the other hand, the two-dimensional limit of our three-dimensional solution provides a curious result. For the case $k = 0$, the frequency of the lowest three-dimensional mode ($n = 1$, $b = +1$) becomes $\omega = (1 - m)\Omega$, which corresponds to the frequency of the two-dimensional wave mode (in two dimensions there is only a single wave mode rather than the countable infinity of modes contained in the three-dimensional case). The frequencies of all the higher three-dimensional modes become $\omega = -m\Omega$ when $k = 0$. Thus, the frequency $\omega = -m\Omega$, the discrete version of the continuous spectrum, is not present in three dimensions, but is present in two dimensions.

Briggs *et al.* (1970) have found that if $d\Omega/dr$ is everywhere less than but not equal to zero, then there is a continuous spectrum for the two-dimensional initial value problem. Our results for the Ω = *constant* case do not conflict with this result. However, it would appear that if one solved the three-dimensional initial value problem for a case having $d\Omega/dr < 0$ everywhere, then the solution would necessarily contain a continuous spectrum in order to reproduce the correct behavior in the two-dimensional limit.

We mentioned previously that u_ϕ is not continuous at $r = a$. Rather, the total $\hat{\boldsymbol{\phi}}$-directed velocity is continuous at $r = a + \delta a$. This gives, to first order in perturbed quantities,

$$\Omega[a + \delta a(\phi)] + u_\phi^i|_{r=a} = \frac{\Omega a^2}{a + \delta a(\phi)} + u_\phi^o|_{r=a}, \tag{2.43}$$

where $\delta a(\phi)$ is the tube's perturbed radius written explicitly as a function of ϕ. This

https://doi.org/10.1017/S0022112097005958 Published online by Cambridge University Press

equation can be solved to give the radius perturbation

$$\delta a(\phi) = \frac{1}{2\Omega}(u^o_\phi - u^i_\phi)|_{r=a}. \tag{2.44}$$

The radius perturbation will be an important quantity as it shows the core deformations that a vortex tube undergoes due to Kelvin wave events.

3. An $m = 0$ example

In this Section, we present an example of the special case $m = 0$ using the formalism of the previous Section. Waves with $m = 0$ are axisymmetric and are free of the retrograde/cograde degeneracy.

The example we show is an initial increase in the $\hat{\boldsymbol{z}}$-directed vorticity. The increase is localized in z by a Gaussian function, is independent of r, and is taken to be

$$\omega_z(0) = \frac{2\Omega\epsilon}{\sigma(2\pi)^{1/2}}\mathrm{e}^{-z^2/(2\sigma^2)}, \tag{3.1}$$

where σ is the axial width of the perturbation, and where ϵ is a constant much less than σ so that the perturbed vorticity is much less than the unperturbed vorticity $2\Omega\hat{\boldsymbol{z}}$. We take the vortex tube to be initially untwisted:

$$\omega_\phi(0) = 0. \tag{3.2}$$

Using $\nabla \cdot \boldsymbol{\omega} = 0$, we find the initial radial component of vorticity to be

$$\omega_r(0) = \frac{\Omega\epsilon}{\sigma(2\pi)^{1/2}}\frac{rz}{\sigma^2}\mathrm{e}^{-z^2/(2\sigma^2)}. \tag{3.3}$$

The initial velocity perturbation due to the initial vorticity perturbation is in the $\hat{\boldsymbol{\phi}}$-direction only and is given by

$$u^i_\phi(0) = \frac{\Omega r\epsilon}{\sigma(2\pi)^{1/2}}\mathrm{e}^{-z^2/(2\sigma^2)}, \tag{3.4}$$

$$u^o_\phi(0) = 0, \tag{3.5}$$

$$u^i_r(0) = u^o_r(0) = u^i_z(0) = u^o_z(0) = 0. \tag{3.6}$$

Using (2.44), we find the initial perturbation in the tube's radius to be

$$\frac{\delta a}{a}(0) = \frac{-\epsilon}{2\sigma(2\pi)^{1/2}}\mathrm{e}^{-z^2/(2\sigma^2)}. \tag{3.7}$$

This last expression gives a clearer picture of the initial perturbation of the vortex tube. It is a pinch in the radius of the tube localized around $z = 0$. The vortex lines are untwisted and depart radially from their otherwise straight $\hat{\boldsymbol{z}}$-directed courses to account for the changing radius of the tube.

Fourier transforming (3.1)–(3.3) in z and substituting the results into (A 7) and (A 10) of Appendix A, we find

$$F(0) = \mathrm{i}k\frac{4\Omega^2\epsilon}{s^2}\mathrm{e}^{-\sigma^2k^2/2}, \tag{3.8}$$

$$G(0) = \frac{-2\Omega^2\epsilon r}{\xi^2 s^2}\mathrm{e}^{-\sigma^2k^2/2}. \tag{3.9}$$

https://doi.org/10.1017/S0022112097005958 Published online by Cambridge University Press

The function $g(r)$ is found from (2.30) and is

$$g(r) = \frac{F(0)}{k^2\xi^2} = \mathrm{i}k\frac{4\Omega^2\epsilon}{k^2\xi^2 s^2}\mathrm{e}^{-\sigma^2k^2/2}, \tag{3.10}$$

where the Bessel function integral that was performed may be found in Abramowitz & Stegun (1964).

Using (3.8)–(3.10) in (2.41)–(2.42), the $\hat{z}$-directed flow field is found to be

$$u_z^i = 2\mathrm{i}\sum_{n=1}^{\infty}\frac{J_0(k\xi_n r)}{J_0(k\xi_n a)}C_n\sin(\omega_n t)\mathrm{e}^{-\mathrm{i}kz}, \tag{3.11}$$

$$u_z^o = 2\mathrm{i}\sum_{n=1}^{\infty}\frac{K_0(kr)}{K_0(ka)}C_n\sin(\omega_n t)\mathrm{e}^{-\mathrm{i}kz}, \tag{3.12}$$

where

$$C_n = \frac{\epsilon\mathrm{e}^{-\sigma^2k^2/2}\left[\dfrac{\omega_n}{k}\dfrac{J_0'(k\xi_n a)}{k\xi_n a J_0(k\xi_n a)} + \dfrac{\omega_n}{2k}\right]}{\left[1 + \dfrac{2J_0'(k\xi_n a)}{k\xi_n a J_0(k\xi_n a)} + \left(\dfrac{J_0'(k\xi_n a)}{J_0(k\xi_n a)}\right)^2\right]}, \tag{3.13}$$

and where ξ_n and ω_n are given by (2.21) and (2.20) respectively with $m = 0$.

To return to a function of z instead of k, we invert the Fourier transform. Noting the antisymmetry in k in the above expressions, this can be written as

$$u_z(r,z,t) = \frac{1}{2\pi}\int_{-\infty}^{\infty}u_z(r,k,t)\mathrm{e}^{-\mathrm{i}kz}\mathrm{d}k = \frac{-\mathrm{i}}{\pi}\int_0^{\infty}u_z(r,k,t)\sin(kz)\mathrm{d}k. \tag{3.14}$$

As a final answer, we arrive at

$$u_z^i = \frac{2}{\pi}\int_0^{\infty}\sum_{n=1}^{\infty}\frac{J_0(k\xi_n r)}{J_0(k\xi_n a)}C_n\sin(\omega_n t)\sin(kz)\mathrm{d}k, \tag{3.15}$$

$$u_z^o = \frac{2}{\pi}\int_0^{\infty}\sum_{n=1}^{\infty}\frac{K_0(kr)}{K_0(ka)}C_n\sin(\omega_n t)\sin(kz)\mathrm{d}k. \tag{3.16}$$

In understanding the flow's evolution, we will find several quantities helpful. Since they are all to be derived trivially from (3.15) and (3.16), we do not write them explicitly, but rather only refer to the expressions to be used in deriving them. The first are the vorticity components ω_z and ω_ϕ, where ω_z is found immediately from (3.15) and (C 3), and ω_ϕ is found from (3.15), (2.11) and (C 3). The next quantity is the change in ω_z due to stretching/scrunching.† Stretching/scrunching is the only source of ω_z and is given by $\partial\omega_z/\partial t = 2\Omega\partial v_z/\partial z$, which is found directly from (3.15). Finally, we require δa, the change in radius of the tube; this is found from (3.15), (2.11), (2.15) and (2.44).

For the remainder of this Section, we discuss the specific case of $\sigma = a$. This choice is motivated by the typical scale of perturbations found in the gravity wave simulations discussed in companion papers (Andreassen *et al.* 1997; Fritts *et al.* 1997).

† Use of the term 'stretching' to describe an increase in the local vorticity from flow divergence in the direction of the vorticity is well established. We will use the term 'scrunching' to denote the opposite, i.e. a decrease in the local vorticity from flow convergence along the vorticity direction.

https://doi.org/10.1017/S0022112097005958 Published online by Cambridge University Press

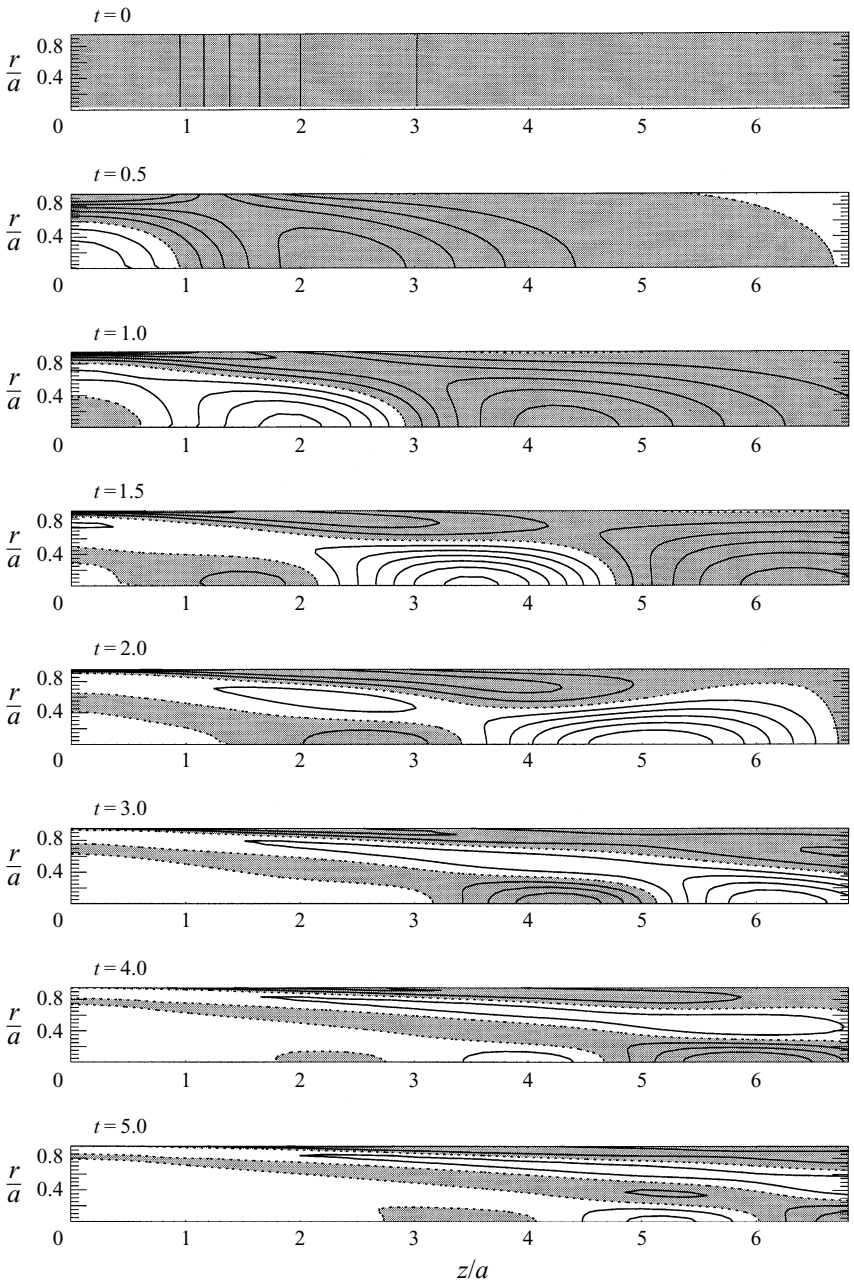


FIGURE 1. ω_z for the $m = 0$ wave packet having $\sigma = a$. The contour levels are held fixed in time and are at intervals of 0.1. In this and similar figures, a dotted line separates the shaded positive contours from the unshaded negative contours.

The evolutions of ω_z, ω_ϕ and $\partial\omega_z/\partial t$ for this case are shown in figures 1, 2 and 3 using contour plots in the (z,r)-plane at sequential instants of time. The contour levels are held fixed with time and are given in the figure captions. The time steps are normalized to the rotational timescale of the unperturbed vortex, so that $t_{norm} = \Omega/2\pi$. Consider first the initial state at $t = 0$: ω_z varies in z as a Gaussian function, but does not vary

https://doi.org/10.1017/S0022112097005958 Published online by Cambridge University Press

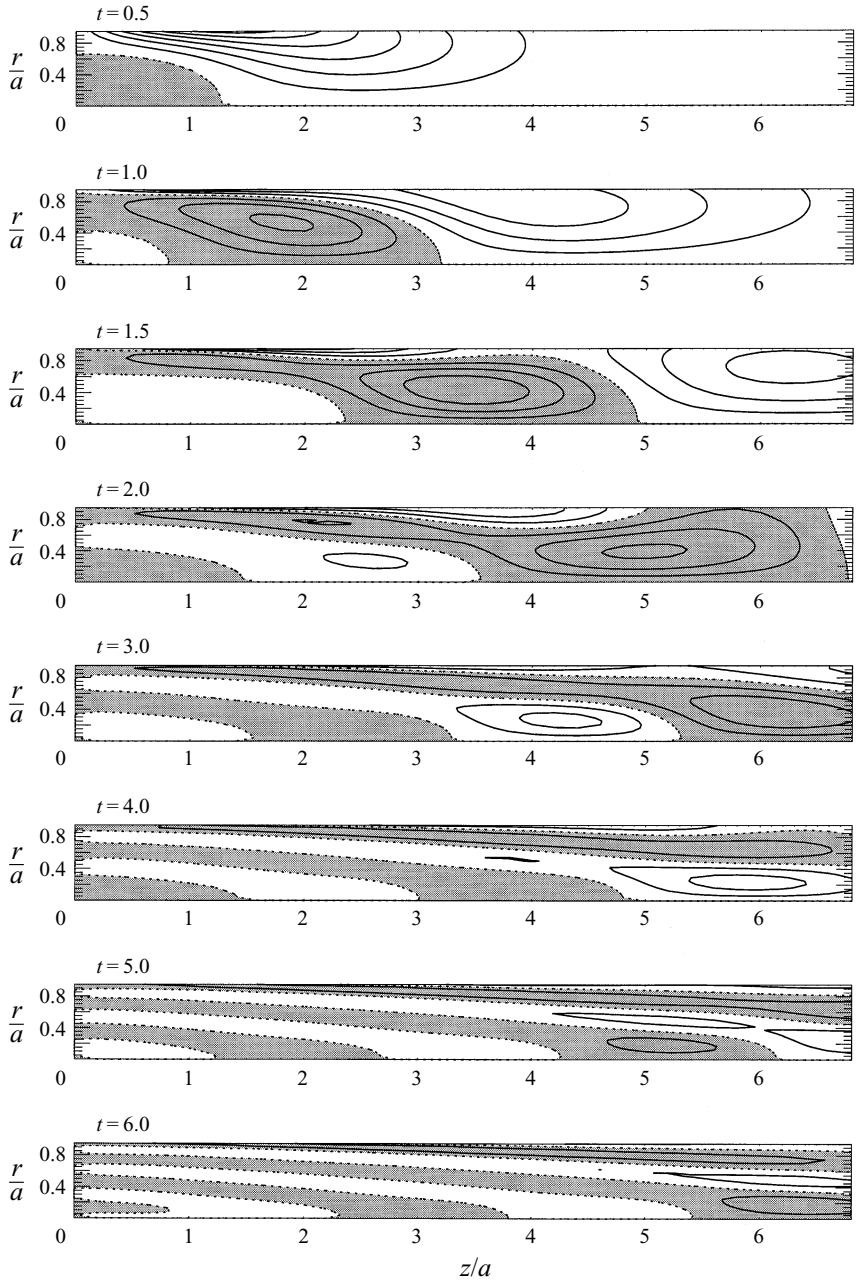


FIGURE 2. ω_ϕ for the $m = 0$ wave packet having $\sigma = a$. The contour levels are held fixed in time and are at intervals of 0.1.

in r; both ω_ϕ and $\partial\omega_z/\partial t$ are zero at $t = 0$ and so are not shown. It will be important to note that ω_z is directly linked to the angular velocity u_ϕ via $\omega_z = \partial u_\phi/\partial r$. So, u_ϕ initially varies linearly in r and varies as a Gaussian in z.

Now, a z-varying u_ϕ is a differential rotation of the vortex tube: different locations along the tube but at the same radius rotate around the tube at different rates. The vorticity lines comprising the tube are twisted into helices by this differential rotation.

https://doi.org/10.1017/S0022112097005958 Published online by Cambridge University Press

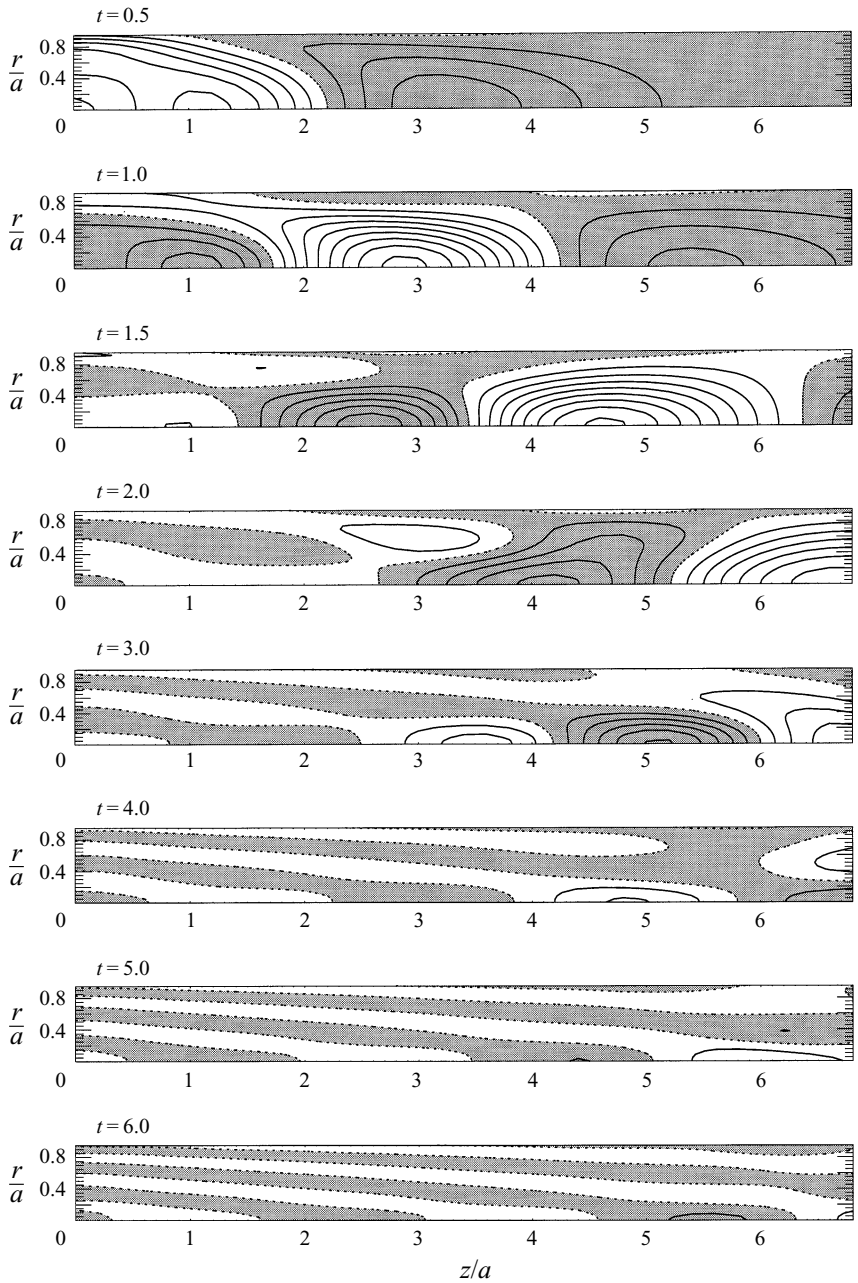


FIGURE 3. The stretching/scrunching of ω_z, $\partial\omega_z/\partial t$, for the $m = 0$ wave packet having $\sigma = a$. The contour levels are held fixed in time and are at intervals of 0.05.

This effect is clearly seen in figure 2: ω_ϕ, which serves as an indication of the twist or helicity in the vorticity lines, has changed from zero at $t = 0$ to negative at $t = 0.5$ (except for being slightly positive at low r and z) due to the differential rotation.

A ω_ϕ induces a flow in the (z,r)-plane via $\omega_\phi = \partial u_r/\partial z - \partial u_z/\partial r$; we will be interested only in the axial ($\hat{\boldsymbol{z}}$-directed) component of this flow. So, a twist in the vorticity lines induces an axial flow, and moreover a z-varying twist in the vorticity

https://doi.org/10.1017/S0022112097005958 Published online by Cambridge University Press

lines induces a z-varying axial flow. Such a z-varying axial flow leads to a production of ω_z by a stretching/scrunching of the vorticity lines; this is shown in figure 3. Focusing on $t = 0.5$, the stretching/scrunching source is negative at small z and positive at large z, corresponding to an axial flow in the $-\hat{z}$-direction which peaks at about $z \simeq 2.25$ and decreases both inward and outward from there. Finally, the stretching/scrunching changes ω_z and accounts for the form of ω_z at $t = 0.5$; ω_z is seen to decrease at the origin and increase at larger z.

This evolution has a signature in the core size of the vortex tube which follows from the fact that the total circulation of the vortex tube must be constant. If the perturbation in ω_z is positive, then the total ω_z is greater than the unperturbed value and the core must be thinner to preserve the constant circulation. Of course the opposite holds true if the perturbation in ω_z is negative. Figure 4 shows the evolution of δa, the perturbation in the radius of the vortex tube. Note, in particular, the correspondence between δa in figure 4 and ω_z in figure 1.

To review, the initial time behaviour can be understood by the following sequence of events. A z-varying ω_z creates a differential rotation along a vortex tube. The differential rotation twists the vorticity lines and creates a ω_ϕ. The ω_ϕ induces a u_z which varies with z if ω_ϕ varies with z. Finally the z-varying u_z stretches/scrunches ω_z. In particular, regions of high ω_z undergo a decrease in ω_z and regions of low ω_z undergo an increase. This same sequence of events has been described previously by Melander & Hussain (1994) in a numerical calculation of a perturbed vortex tube. Specifically, they study a tube with a vorticity distribution which is very close to a Gaussian. Imposing an initial core-radius pinch that is periodic in z and is not small compared to the unperturbed tube radius, they find that the differential rotation of the tube and the resulting meridional flow lead to an oscillation in the tube's core radius. They note the wave-like character of the oscillation, but do not discuss its relation to Kelvin waves.

The crucial point in this regard is that the dynamical sequence of events outlined above is the same as that which causes the propagation of $m = 0$ Kelvin vortex waves. That is, a single wave mode propagates by alternately twisting/untwisting the vortex lines of the tube. The restoring mechanism of the wave is the coupling between this twist and the axial flow which stretches/scrunches ω_z and changes the differential rotation. With this in mind, one might think of $m = 0$ Kelvin waves as 'twist' waves. Figure 5 shows ω_z, ω_ϕ and $\partial\omega_z/\partial t$ for the lowest-(radial) order wave mode with $k = 1/a$. As is expected, ω_ϕ leads $\partial\omega_z/\partial t$ by $\pi/2$; it is $\partial\omega_\phi/\partial z$ which provides for $\partial u_z/\partial z$ and the consequent $\partial\omega_z/\partial t$ from stretching/scrunching. Note also that the stretching/scrunching $\partial\omega_z/\partial t$ leads ω_z by $\pi/2$, as expected. Finally, $\partial\omega_\phi/\partial t$ lags ω_z by $\pi/2$, since the z-variation in ω_z causes the twisting of the lines described by $\partial\omega_\phi/\partial t$. Thus the events described in the previous paragraphs may simply be understood as the propagation of Kelvin waves away from the site of the initial perturbation. This is especially clear when one notes the motion of the phase fronts in figures 1–3 as time progresses and recognizes that the phase relationship between ω_z, ω_ϕ and $\partial\omega_z/\partial t$ is the same in figures 1–3 as in figure 5. The decomposition of a vortex tube perturbation into Kelvin waves is not just for convenience: Kelvin waves are the fundamental oscillation modes of the vortex tube, and they provide a straightforward physical understanding of the evolution of any initial perturbation.

Consider next the late-time evolution shown in figures 1–3. The perturbation has grown weaker, but more importantly has also changed to smaller axial scales and has developed considerable radial structure. The Kelvin wave picture provides a simple explanation for this. As noted in § 2, for a given axial wavelength there is a multiplicity of modes with different radial structures and different frequencies. As an example,

https://doi.org/10.1017/S0022112097005958 Published online by Cambridge University Press

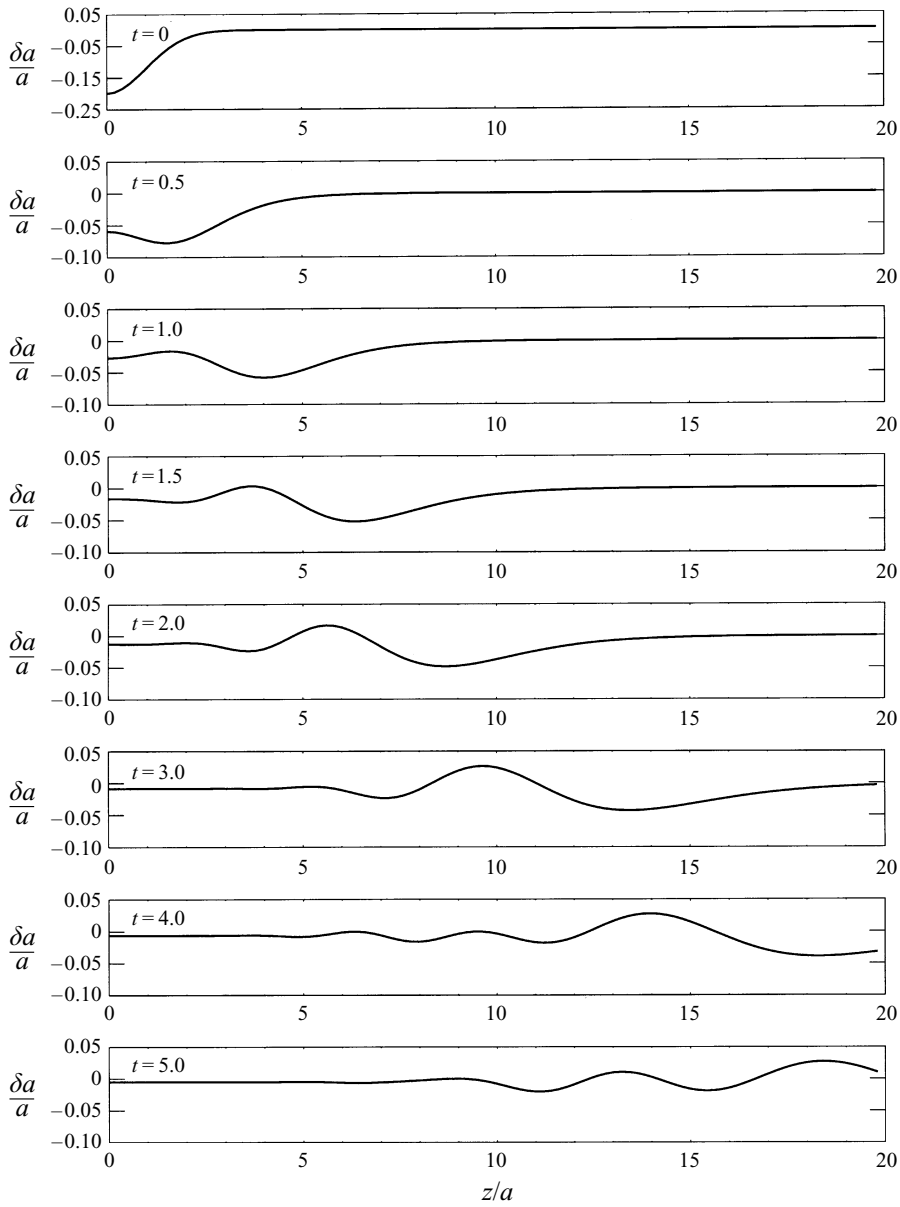


FIGURE 4. Perturbation in radius, δa, for the $m = 0$ wave packet having $\sigma = a$.

figure 6 shows the radial structure of the first four modes for $k = 1/a$; one sees that the nth mode has n zeros so that modes with higher n have more radial structure. The different modes also have different group velocities, as can be seen in figure 7. One finds that the low-n wave modes (those with less radial structure) propagate faster than the high-n wave modes (those with more radial structure). Furthermore, wave modes with longer wavelengths propagate faster than those with shorter wavelengths. The late-time evolution shown in figures 1–3, then, is simply a result of wave dispersion. At late times, the faster modes (those with longer wavelength and less radial structure) have propagated away leaving the slower modes (those with shorter wavelength and

https://doi.org/10.1017/S0022112097005958 Published online by Cambridge University Press

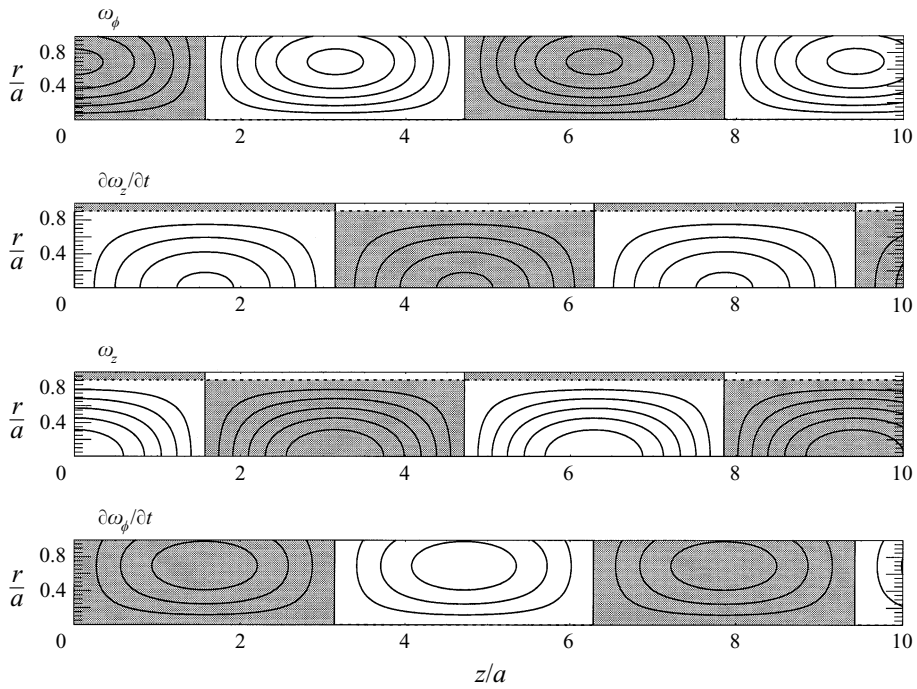


FIGURE 5. Contour plots of ω_z, ω_ϕ and $\partial\omega_z/\partial t$ for the $n = 1$ $m = 0$ wave mode with $k = 1/a$ at a single instant in time. The contour levels are every 0.33.

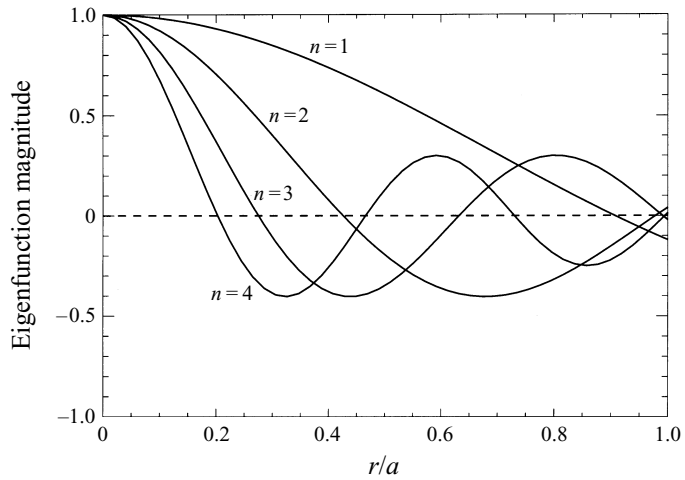


FIGURE 6. Radial variation of the first four $m = 0$ wave modes $J_0(k\xi_n r)$ for $k = 1/a$.

more radial structure) behind. Finally, in the series expansion (3.15) one finds that the low-n modes have a much larger amplitude than the high-n modes, accounting for the dramatic decrease in the magnitude of the perturbations with time in figures 1–3.

The dispersion of Kelvin waves may shed light on the low-enstrophy bubble found by Melander & Hussain (1994) in the centre of the core of their vortex tube. Note in their figure 6 that the minima in the wave packets appear to follow the maxima (e.g. in figure 6*c* and 6*g*) and that the minima and maxima are located at the centre of the

https://doi.org/10.1017/S0022112097005958 Published online by Cambridge University Press

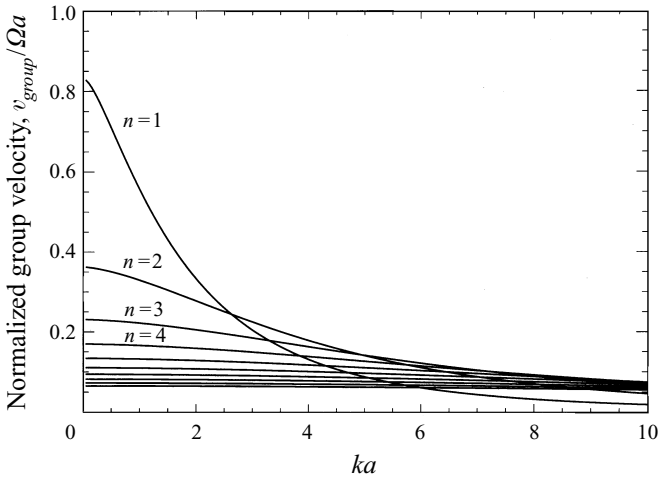


FIGURE 7. Group velocities of the first ten $m = 0$ wave modes as functions of the axial wavenumber k.

vortex core. This behaviour is similar to that shown in our figure 1. At early times the various wave modes disperse so that minima and maxima are formed near the centre of the vortex core, with the minima following the maxima (note $t = 1.0$ and $t = 1.5$ in particular). With a sufficiently high viscosity, the higher-order modes with more radial structure will be viscously damped, so that only this lowest-order mode remains. We interpret the low-enstrophy bubble in Melander & Hussain's figure 6(*i*) to be the superposition of the two minima of the two individual wave packets.

4. An $m = 1$ example

In this section, we present an example of $m = 1$ Kelvin waves. Wave modes with $m = 1$ are particularly interesting as they are the only wave mode that can displace the centre of the vortex tube. In fact, a single $m = 1$ wave mode twists the vortex tube into a propagating helix.

Our example is a vortex tube with an initial displacement in the $\hat{\boldsymbol{x}}$-direction, where x is related to the cylindrical coordinates by the usual formula: $x = r\cos\phi$. The displacement is localized around $z = 0$ by a Gaussian function. To represent this, we take

$$\omega_x(0) = 2\Omega\frac{\epsilon}{\sigma(2\pi)^{1/2}}\frac{\partial}{\partial z}\mathrm{e}^{-z^2/(2\sigma^2)}, \tag{4.1}$$

$$\omega_y(0) = \omega_z(0) = 0. \tag{4.2}$$

As before, σ is the axial width of the perturbation, and ϵ is a constant much less than σ so that the perturbed vorticity is much less than the unperturbed vorticity $2\Omega\hat{\boldsymbol{z}}$. Outside the vortex tube, the flow is taken to be potential; there is no need to specify its initial state explicitly since the specification of the vorticity perturbation of the tube uniquely determines the external potential flow.

In cylindrical coordinates, we find

$$\omega_r(0) = \omega_x(0)\cos\phi, \tag{4.3}$$

$$\omega_\phi(0) = -\omega_x(0)\sin\phi. \tag{4.4}$$

https://doi.org/10.1017/S0022112097005958 Published online by Cambridge University Press

One can show from the accompanying radius perturbation that this vorticity perturbation leads to a displacement of the tube's centre given by

$$\boldsymbol{d} = \frac{\epsilon \hat{\boldsymbol{x}}}{\sigma(2\pi)^{1/2}} \mathrm{e}^{-z^2/(2\sigma^2)}. \tag{4.5}$$

Using (4.3) and (4.4), it is straightforward to show from (A 7) that $F(0) = 0$, and consequently $g(r) = 0$. From (A 10), $G(0)$ is found to be

$$G(0) = \begin{cases} \dfrac{-\mathrm{i}\epsilon\Omega(s + 3\mathrm{i}\Omega)}{\xi^2(s + \mathrm{i}\Omega)^2} \mathrm{e}^{-\sigma^2k^2/2}, & m = 1 \\ \dfrac{\mathrm{i}\epsilon\Omega(s - 3\mathrm{i}\Omega)}{\xi^2(s - \mathrm{i}\Omega)^2} \mathrm{e}^{-\sigma^2k^2/2}, & m = -1, \end{cases} \tag{4.6}$$

where we have separated the $m = \pm 1$ components. Substituting this result into (2.41) and (2.42) and summing over $b = \pm 1$, we find, after simplification,

$$u_z^i = 2\mathrm{i} \sum_{n=0}^{\infty} \left(C_n^+ \frac{J_1(k\xi_n^+ r)}{J_1(k\xi_n^+ a)} \sin(\phi + \omega_n^+ t) + C_n^- \frac{J_1(k\xi_n^- r)}{J_1(k\xi_n^- a)} \sin(\phi + \omega_n^- t) \right), \tag{4.7}$$

$$u_z^o = 2\mathrm{i} \sum_{n=0}^{\infty} \left(C_n^+ \frac{K_1(kr)}{K_1(ka)} \sin(\phi + \omega_n^+ t) + C_n^- \frac{K_1(kr)}{K_1(ka)} \sin(\phi + \omega_n^- t) \right), \tag{4.8}$$

where

$$C_n^{\pm} = \frac{\mp \epsilon \mathrm{e}^{-\sigma^2k^2/2} \left[\dfrac{(\omega_n^{\pm} + 3\Omega)(\omega_n^{\pm} + \Omega)}{4\Omega ka} \right]}{1 - \dfrac{1}{(k\xi_n^{\pm} a)^2} + \dfrac{2J_1'(k\xi_n^{\pm} a)}{k\xi_n^{\pm} a J_1(k\xi_n^{\pm} a)} + \left(\dfrac{J_1'(k\xi_n^{\pm} a)}{J_1(k\xi_n^{\pm} a)} \right)^2 \pm \dfrac{(\xi_n^{\pm})^2 + 2}{(k\xi_n^{\pm} a)^2((\xi_n^{\pm})^2 + 1)^{1/2}}}, \tag{4.9}$$

and where $\xi_n^{\pm}$ and $\omega_n^{\pm}$ are given by (2.21) and (2.20) respectively with $m = 1$ and $b = \pm 1$.

The z-dependence is returned by performing the inverse Fourier transform, which, noting the antisymmetry in both (4.7) and (4.8) as $k \to -k$, is given by (3.14). We obtain as a final answer

$$u_z^i = \frac{2}{\pi} \int_0^{\infty} \sum_{n=1}^{\infty} \left(C_n^+ \frac{J_1(k\xi_n^+ r)}{J_1(k\xi_n^+ a)} \sin(\phi + \omega_n^+ t) + C_n^- \frac{J_1(k\xi_n^- r)}{J_1(k\xi_n^- a)} \sin(\phi + \omega_n^- t) \right) \sin(kz)\mathrm{d}k, \tag{4.10}$$

$$u_z^o = \frac{2}{\pi} \int_0^{\infty} \sum_{n=1}^{\infty} \left(C_n^+ \frac{K_1(kr)}{K_1(ka)} \sin(\phi + \omega_n^+ t) + C_n^- \frac{K_1(kr)}{K_1(ka)} \sin(\phi + \omega_n^- t) \right) \sin(kz)\mathrm{d}k. \tag{4.11}$$

We now go on to discuss the case $\sigma = a$ in detail. As in the previous Section, this choice is made to provide a rough correspondence with the breaking gravity wave simulations discussed in our companion papers (Andreassen *et al.* 1997; Fritts *et al.* 1997). To display the evolution, we will use the perturbation in the radius of the vortex tube from which one finds the displacement of the centre of the tube. The radius perturbation is found from (4.10), (4.11), (2.11), (2.15) and (2.44). Figure 8 shows the evolution of the surface of the tube for early times while Figure 9 shows the evolution for later times. In these figures, we have made the wave amplitude large so that it can

https://doi.org/10.1017/S0022112097005958 Published online by Cambridge University Press

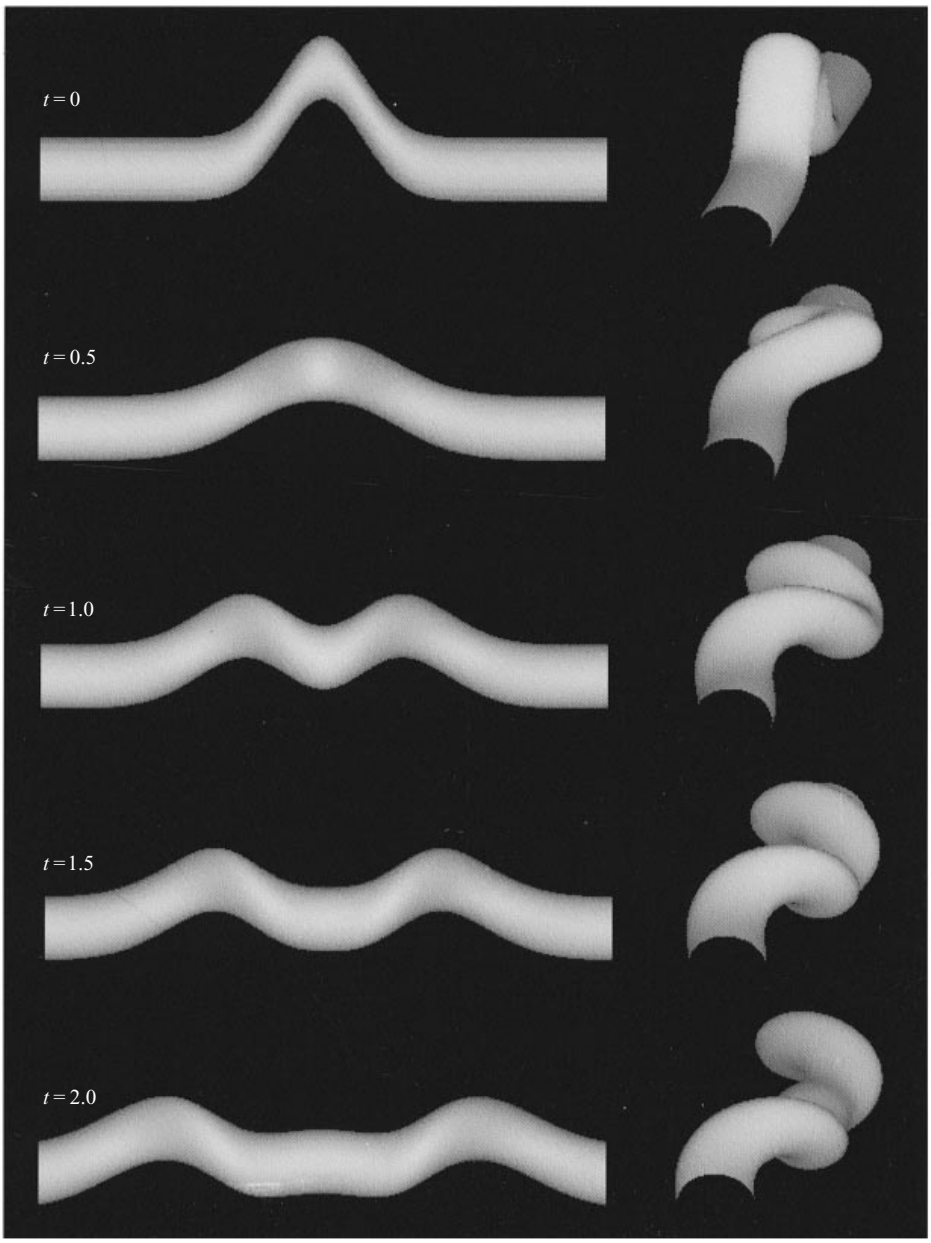


FIGURE 8. Early time evolution of the surface of a vortex tube under the influence of an $m = 1$ wave packet having $\sigma = a$. Two views are shown: a side view with $\hat{\boldsymbol{z}}$ pointing to the left, and a rotated view with $\hat{\boldsymbol{z}}$ rotated toward the viewer and slightly downward. The range of z shown is $-7a \leqslant z \leqslant 7a$.

be conveniently seen; this large amplitude is inconsistent with the linearized equations of motion and is for display only. The time steps in figures 8 and 9 are normalized to the rotational timescale of the unperturbed vortex, so that $t_{norm} = \Omega/2\pi$.

Consider first the early-time evolution shown in figure 8, which is side views of the tube for which $\hat{\boldsymbol{z}}$ points to the left and rotated views for which $\hat{\boldsymbol{z}}$ is rotated toward

https://doi.org/10.1017/S0022112097005958 Published online by Cambridge University Press

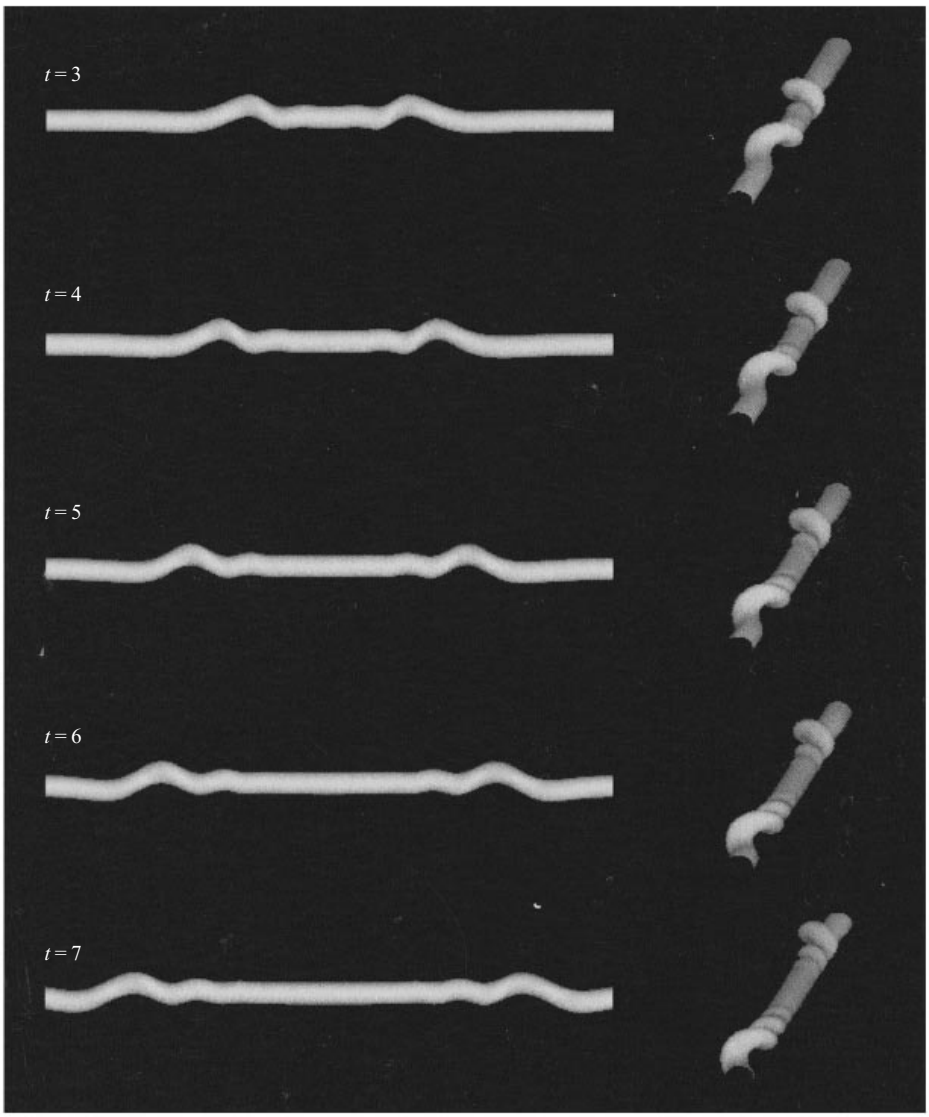


FIGURE 9. As figure 8 but at later times. The range of z shown is $-20a \leqslant z \leqslant 20a$.

the viewer and slightly downward. As described in (4.5), the tube is initially deflected in the $\hat{\boldsymbol{x}}$-direction near the origin. As time proceeds, the deflection bends toward $-\hat{\boldsymbol{y}}$, and proceeds to rotate completely around the tube. At the last time in this sequence, the perturbation has started to form two helices: a right-handed helix travelling in the $+\hat{\boldsymbol{z}}$-direction and a left-handed helix travelling in the $-\hat{\boldsymbol{z}}$-direction.†

This behaviour is due to the advection of the vortex tube by its own velocity field. We digress momentarily to discuss this effect in detail, which is most easily

† The handedness of a helix is found as follows. Point the thumb of one's right hand in the direction of the unperturbed vorticity and curl one's fingers slightly. If one's fingers then point in the direction of the $\hat{\boldsymbol{\phi}}$-directed vorticity, the helix is right-handed. If one's fingers point in the opposite direction of the $\hat{\boldsymbol{\phi}}$-directed vorticity, the helix is left-handed.

https://doi.org/10.1017/S0022112097005958 Published online by Cambridge University Press

demonstrated in the thin-core (or long-wavelength) limit. It can be shown that a curved vortex tube with a thin core advects itself in a direction given by $\hat{\boldsymbol{R}} \times \hat{\boldsymbol{\omega}}$ where $\hat{\boldsymbol{R}}$ is the direction of the radius of curvature (see e.g. Batchelor 1967, pp. 510–511). The self-advection has a magnitude given by $\kappa/4\pi R \ln(b/R)$ where κ is the circulation of the vortex, R is the radius of curvature and b is the core radius; this expression assumes that the radius of curvature is large compared to the core size of the vortex tube. A simple example of this is a thin-cored vortex ring which advects itself in a direction perpendicular to the plane of the ring and with a speed given by $\kappa/4\pi R \ln(b/R)$. One generally thinks of the the curvature of the ring as causing the advection, since the advection speed becomes small if the radius of curvature is made large. Still, the fundamental effect is simply the advection of the vortex ring by its own velocity field. Saffman (1992) has shown that this approximation for the curvature self-advection and the accompanying vortex tilting reproduces the dispersion relation of the $m = 1$, $n = 1$ Kelvin wave in the long-wavelength limit; thus such a Kelvin wave propagates due to self-advection.

Now, returning to figure 8 we use the long-wavelength results for the curvature self-advection as a guide in interpreting the evolution. At $t = 0$, $\hat{\boldsymbol{R}} \times \hat{\boldsymbol{\omega}} = -\hat{\boldsymbol{y}}$, which gives the direction of the initial bending of the deflection. At later times, the direction of the radius of curvature precesses about the tube (clockwise in the rotated views of figure 8), wrapping the tube into two helices: a right-handed helix in the $+\hat{\boldsymbol{z}}$ part of the tube and a left-handed helix in the $-\hat{\boldsymbol{z}}$ part of the tube. These helices propagate outward along the vortex tube, with the right-handed helix propagating in the $+\hat{\boldsymbol{z}}$-direction and the left-handed helix propagating in the $-\hat{\boldsymbol{z}}$-direction. The direction of propagation of each helix may be understood with the curvature self-motion in mind. Thus, the evolution shown in figure 8 is the launching of two $m = 1$ helical wave packets away from the site of the original perturbation.

Figure 9 shows the same views at later times, but with a greater length of the vortex tube displayed. The two wave packets with right-handed and left-handed helicity propagating in the $\pm\hat{\boldsymbol{z}}$-direction respectively are clearly shown. It is also apparent that the packets are dispersing as they propagate. To understand this, consider the group velocity shown in figure 10. The group velocities for all but the lowest-order mode behave in an ordered fashion with the higher-order modes propagating slower than the lower-order modes, and high-wavenumber modes propagating slower than low-wavenumber modes; this is the same as was found for the $m = 0$ modes. However, the $n = 1$ mode behaves curiously with its group velocity increasing to a maximum at $ka \simeq 0.5$ and decreasing thereafter. The wave packets shown in figures 8 and 9 are composed almost entirely of $n = 1$ waves, so we concentrate on this case. The effect of the maximum of the $n = 1$ group velocity is to set the axial scale of the initial wave packet to be that of the fastest wave, i.e. $ka \simeq 0.5$. Waves with wavelengths shorter or longer than this are left behind. In particular, waves with shorter wavelengths can be seen separating out at later times in figure 9. Waves with longer wavelengths are also present, but are difficult to see since they deflect large lengths of the tube uniformly. In addition to the axial dispersion, there is angular dispersion as well, since different modes rotate about the tube at different rates.

5. An $m = 2$ example

In this section, we present an example of $m = 2$ Kelvin waves. Wave modes of $m > 1$ cause non-axisymmetric core deformations on the vortex tube without displacing the

https://doi.org/10.1017/S0022112097005958 Published online by Cambridge University Press

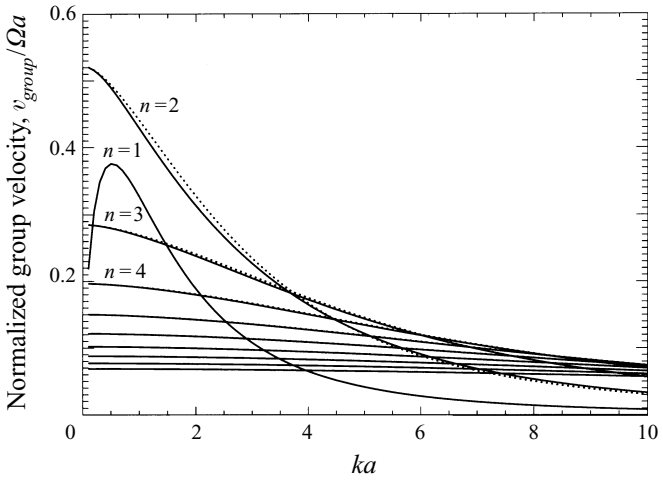


FIGURE 10. Group velocities of the first ten $m = 1$ wave modes as functions of the axial wavenumber k. Solid lines correspond to retrograde $b = +1$ modes; dotted lines correspond to cograde $b = -1$ modes. For the higher-order modes, the $b = \pm 1$ modes are closely aligned and cannot be distinguished.

vortex tube's centre. A single mode with $m > 1$ essentially deforms the tube into a set of m helices all of the same sense and all axially propagating.

For our example, we take a flattening of the vortex core localized in z by a Gaussian function. To achieve this, we let

$$\omega_x(0) = \frac{2\Omega\epsilon}{\sigma(2\pi)^{1/2}} x \frac{\partial e^{-z^2/(2\sigma^2)}}{\partial z}, \tag{5.1}$$

$$\omega_y(0) = \frac{-2\Omega\epsilon}{\sigma(2\pi)^{1/2}} y \frac{\partial e^{-z^2/(2\sigma^2)}}{\partial z}, \tag{5.2}$$

$$\omega_z(0) = 0. \tag{5.3}$$

As in the previous sections, σ is the axial width of the perturbation, and ϵ is a constant much less than σ so that the perturbed vorticity is much less than the unperturbed vorticity $2\Omega\hat{z}$. The external flow is taken to be potential.

In cylindrical coordinates, the initial vorticity is

$$\omega_r(0) = \frac{2\Omega\epsilon}{\sigma(2\pi)^{1/2}} r\cos(2\phi) \frac{\partial e^{-z^2/(2\sigma^2)}}{\partial z}, \tag{5.4}$$

$$\omega_\phi(0) = \frac{-2\Omega\epsilon}{\sigma(2\pi)^{1/2}} r\sin(2\phi) \frac{\partial e^{-z^2/(2\sigma^2)}}{\partial z}. \tag{5.5}$$

The interpretation of the initial perturbation as a localized flattening of the vortex's cross-section follows from the initial radius perturbation of the core, which may be shown to be

$$\delta a(\phi) = \frac{a\epsilon}{\sigma(2\pi)^{1/2}} \cos(2\phi) e^{-z^2/(2\sigma^2)}. \tag{5.6}$$

It is straightforward to show from (A 7), (5.4), and (5.5) that $F(0) = 0$, and so $g(r) = 0$. The initial conditions are then represented only through $G(0)$, which is

https://doi.org/10.1017/S0022112097005958 Published online by Cambridge University Press

found using (A 10) to be

$$G(0) = \begin{cases} \dfrac{-\mathrm{i}\Omega\epsilon r(s+4i\Omega)}{\xi^2(s+2\mathrm{i}\Omega)^2}\mathrm{e}^{-\sigma^2k^2/2}, & m=2 \\ \dfrac{\mathrm{i}\Omega\epsilon r(s-4\mathrm{i}\Omega)}{\xi^2(s-2\mathrm{i}\Omega)^2}\mathrm{e}^{-\sigma^2k^2/2}, & m=-2, \end{cases} \tag{5.7}$$

where we have separated the $m = \pm 2$ parts. Substituting this result into (2.41)–(2.40), and summing over $b = \pm 1$, we find after simplification

$$u_z^i = 2\mathrm{i}\sum_{n=0}^{\infty}\left(C_n^+\frac{J_2(k\xi_n^+ r)}{J_2(k\xi_n^+ a)}\sin(2\phi+\omega_n^+ t) + C_n^-\frac{J_2(k\xi_n^- r)}{J_2(k\xi_n^- a)}\sin(2\phi+\omega_n^- t)\right), \tag{5.8}$$

$$u_z^o = 2\mathrm{i}\sum_{n=0}^{\infty}\left(C_n^+\frac{K_2(kr)}{K_2(ka)}\sin(2\phi+\omega_n^+ t) + C_n^-\frac{K_2(kr)}{K_2(ka)}\sin(2\phi+\omega_n^- t)\right), \tag{5.9}$$

where

$$C_n^{\pm} = \frac{\mp\epsilon\mathrm{e}^{-\sigma^2k^2/2}\left[\dfrac{(\omega_n^{\pm}+2\Omega)(\omega_n^{\pm}+4\Omega)}{4\Omega k}\right]}{1-\dfrac{4}{(k\xi_n^{\pm}a)^2}+\dfrac{2J_2'(k\xi_n^{\pm}a)}{k\xi_n^{\pm}aJ_2(k\xi_n^{\pm}a)}+\left(\dfrac{J_2'(k\xi_n^{\pm}a)}{J_2(k\xi_n^{\pm}a)}\right)^2 \pm \dfrac{2((\xi_n^{\pm})^2+2)}{(k\xi_n^{\pm}a)^2((\xi_n^{\pm})^2+1)^{1/2}}}, \tag{5.10}$$

and where $\xi_n^{\pm}$ and $\omega_n^{\pm}$ are given by (2.21) and (2.20) respectively with $m = 2$ and $b = \pm 1$.

As in the previous sections, the z-dependence is obtained by performing the inverse Fourier transform, which, noting the antisymmetry in both (5.8) and (5.9) as $k \to -k$, is given by (3.14). The final solution is

$$u_z^i = \frac{2}{\pi}\int_0^{\infty}\sum_{n=1}^{\infty}\left(C_n^+\frac{J_2(k\xi_n^+ r)}{J_2(k\xi_n^+ a)}\sin(2\phi+\omega_n^+ t) + C_n^-\frac{J_2(k\xi_n^- r)}{J_2(k\xi_n^- a)}\sin(2\phi+\omega_n^- t)\right)\sin(kz)\mathrm{d}k, \tag{5.11}$$

$$u_z^o = \frac{2}{\pi}\int_0^{\infty}\sum_{n=1}^{\infty}\left(C_n^+\frac{K_2(kr)}{K_2(ka)}\sin(2\phi+\omega_n^+ t) + C_n^-\frac{K_2(kr)}{K_2(ka)}\sin(2\phi+\omega_n^- t)\right)\sin(kz)\mathrm{d}k. \tag{5.12}$$

The remainder of this Section investigates the special case $\sigma = a$. We use the same method of display as in the previous section; the radius perturbation is calculated and used to show the evolution of the tube surface. Figure 11 shows the evolution for early times while figure 12 shows the later times. As in the previous section, we have made the wave amplitude large so that it can be conveniently seen; this amplitude is inconsistent with the linearized equations of motion and is for display only. The amplitude in figure 12 is larger by a factor of 2.5 than that in figure 11. The time steps in both figures are normalized to the rotational timescale of the unperturbed vortex, so that $t_{norm} = \Omega/2\pi$.

Consider first the early time evolution shown in figure 11. As in the previous Section, it shows side views of the tube for which $\hat{\boldsymbol{z}}$ points to the left and rotated views for which $\hat{\boldsymbol{z}}$ is rotated toward the viewer and slightly downward. The tube is initially flattened so that its cross-section in x is thinner than its cross-section in y. With the amplitude of the wave exaggerated, there is a hint of a separation into two

https://doi.org/10.1017/S0022112097005958 Published online by Cambridge University Press

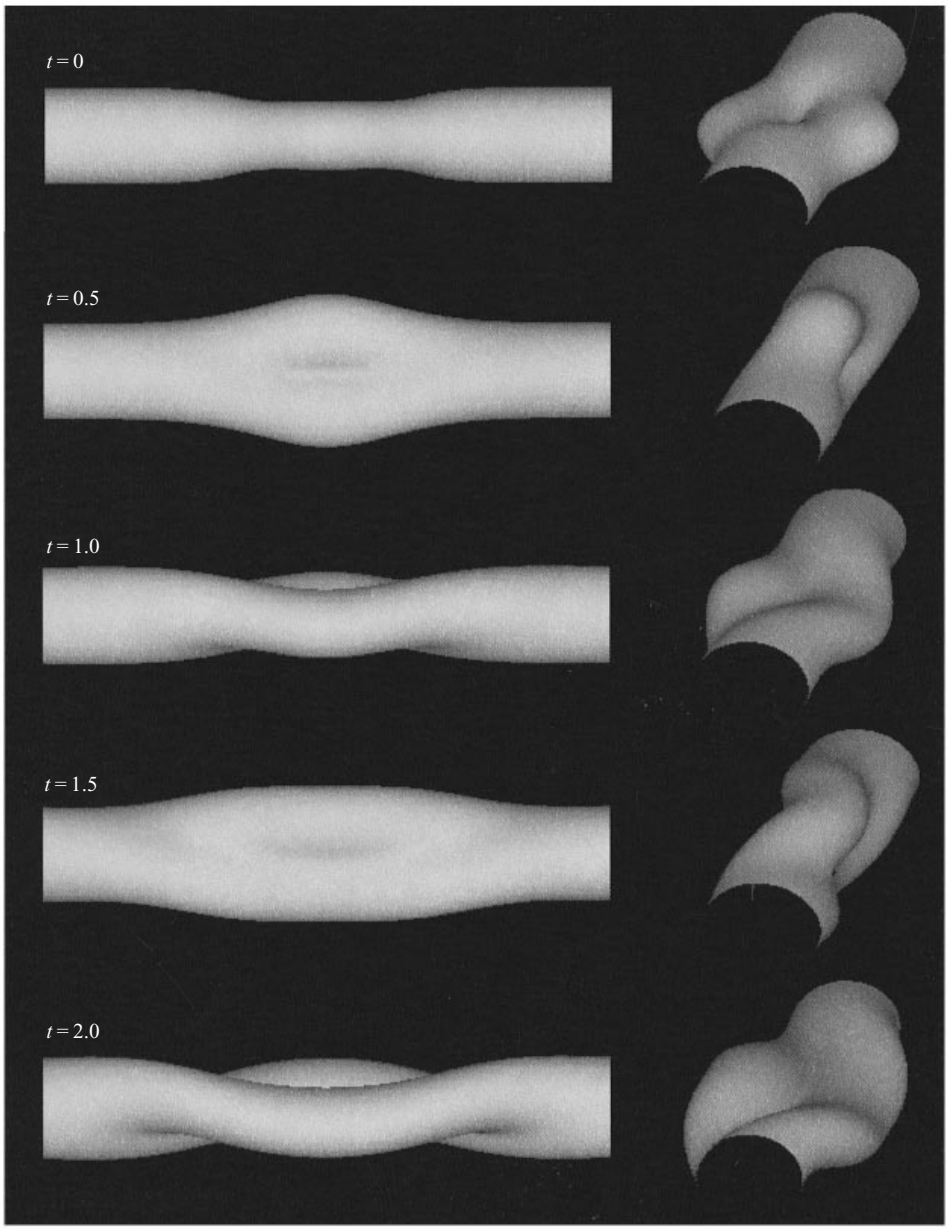


FIGURE 11. Early time evolution of the surface of a vortex tube under the influence of an $m = 2$ wave packet having $\sigma = a$. Two views are shown: a side view with $\hat{\boldsymbol{z}}$ pointing to the left and a rotated view with $\hat{\boldsymbol{z}}$ rotated toward the viewer and slightly downward. The range of z shown is $-7a \leqslant z \leqslant 7a$.

tubes; this is best seen in the rotated view. As time proceeds, two things happen. The most prominent is that the perturbation rotates around the tube in the rotational flow of the vortex. This rotational frequency is half that of the rotational frequency of the unperturbed vortex. The fact that these frequencies are not the same is surprising at first sight, but is the same as has been shown for Kirchhoff's elliptic vortex (Lamb

https://doi.org/10.1017/S0022112097005958 Published online by Cambridge University Press

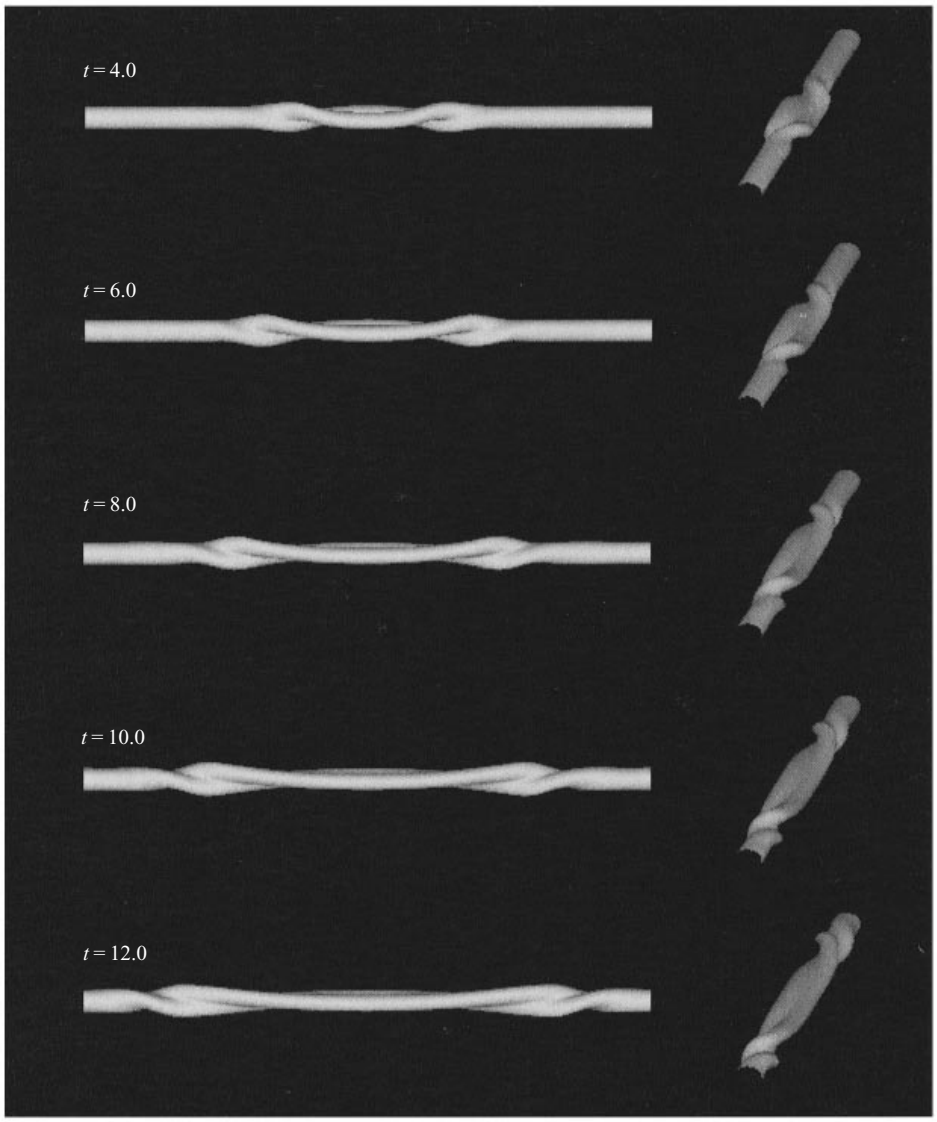


FIGURE 12. As figure 11 but at later times. The range of z shown is $-20a \leqslant z \leqslant 20a$.

1945). The difference in the frequencies is due to the effect of the perturbation on the unperturbed vortex; this resists the unperturbed rotation and leads to a lower net rotation rate. The rotation of the perturbation is apparent in figure 11: in a single time step, the perturbation has rotated through π as is clearly seen.

The second effect that occurs for early times is the same curvature self-motion as was discussed in the previous Section. That is, the perturbation may be thought of as splitting one tube into two tubes, each curved with radii of curvature in the $\pm\hat{\boldsymbol{y}}$-directions, respectively. The curvature self-motion resists the overall rotation so that the most curved regions lag behind the rest of the flow; this is best seen in figure 11 at $t = 1.0$ and $t = 1.5$. A comparison of figure 11 with figure 8 shows the similarity of the evolution of the curvature. The evolution is slower in figure 11

https://doi.org/10.1017/S0022112097005958 Published online by Cambridge University Press

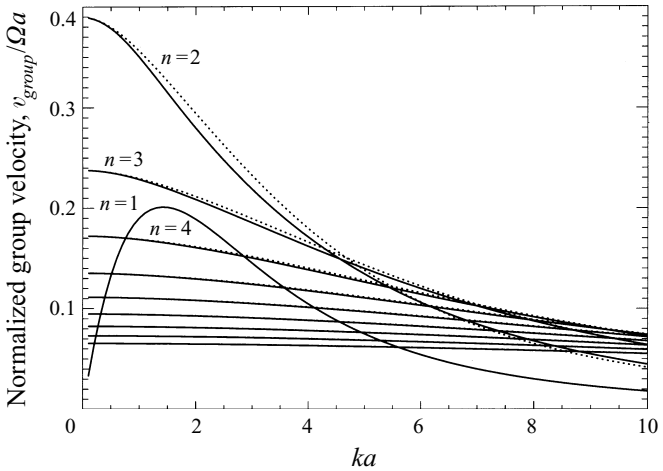


FIGURE 13. Group velocities of the first ten $m = 2$ wave modes as functions of the axial wavenumber k. Solid lines correspond to retrograde $b = +1$ modes; dotted lines correspond to cograde $b = -1$ modes. For the higher-order modes, the $b = \pm 1$ modes are closely aligned and cannot be distinguished.

than in figure 8 since each of the two separated tubes in figure 11 has half the total vorticity while the single tube in figure 8 has all of the total vorticity. The curvature self-motion is reduced proportionally and the evolution is slowed.

At later times, the curvature self-motion has the effect of wrapping the perturbation into two sets of intertwined helices. The first pair has right-handed helicity and propagates in the $+\hat{z}$-direction, while the second pair has left-handed helicity and propagates in the $-\hat{z}$-direction; these are shown prominently in figure 12. The propagation of the helices is due to the self-advection of each curved vortex tube (although complicated by the close proximity of its companion tube), as discussed in the last Section for the $m = 1$ case. Because of this, the sense of the helicity determines the direction of propagation of the helices. The evolution shown in figures 11 and 12 is the launching of two $m = 2$ wave packets from the original site of the perturbation.

As in the previous Sections, the group velocity gives further insight into the dynamics of the wave packets. The group velocities for the lower-order modes are shown in figure 13. As in the $m = 1$ case, all the modes but the lowest-order ones behave in the now-familiar fashion: higher-order modes propagate slower than lower-order modes while modes with higher wavenumbers propagate slower than modes with lower wavenumbers. On the other hand, the lowest-order mode, $n = 1$, has a maximum at $ka \simeq 1.5$. The solutions shown in figures 11 and 12 are composed almost entirely of $n = 1$ modes, so the fastest components of the wave packet have a scale set by the maximum in the group velocity. The wave disperses leaving behind both shorter- and longer-wavelength components. Here, the shorter ones are not much in evidence, but the longer ones are clearly seen as a flattening of the tube which persists to the last times shown. At later times, of course, this too propagates away.

6. Discussion

In this paper we have presented a formal solution to the initial value problem for the evolution of small perturbations on a straight vortex tube of constant vorticity. We find that any initial perturbation of such a tube can be written as a sum of

https://doi.org/10.1017/S0022112097005958 Published online by Cambridge University Press

Kelvin waves, so that any localized disturbance propagates away from its original location as a wave packet. We have presented particular examples for the $m = 0$, $m = 1$, and $m = 2$ cases. The $m = 0$ example is an axisymmetric pinching of the vortex tube's core localized in z. The pinching propagates outward from its original location toward both $\pm\hat{z}$, leaving behind an unperturbed tube. The $m = 1$ example is an initial deflection of the tube at the origin. This deflection winds itself into two helices: a right-handed helix travelling in the $+\hat{z}$-direction and a left-handed helix travelling in the $-\hat{z}$-direction. Finally, the $m = 2$ example is an initial flattening of the core of the tube near the origin. The flattening may be thought of as the tube separating slightly into two tubes near the origin. This disturbance twists itself into two sets of two intertwined helices: a right-handed pair travelling in the $+\hat{z}$-direction and a left-handed pair travelling in the $-\hat{z}$-direction.

In the cases studied, simple physical mechanisms accounting for the propagation of the wave packets were identified. In the $m = 0$ case, this mechanism is the twisting/untwisting of vorticity lines by the differential rotation of an axially varying vortex tube, as has been previously discussed (Melander & Hussain 1994). In the $m = 1$ and $m = 2$ cases, the mechanism is the self-advection of a curved vortex tube. The robustness of these mechanisms is important. Although the results of the present paper have been derived for the special case of small perturbations on a straight vortex tube of constant vorticity, the physical mechanisms providing for the propagation of the disturbances do not depend on the particular distribution of vorticity within the tube or the assumption of linearity. The propagation of disturbances in the form of twist waves along vortex tubes should be a generic feature which is independent of the form of the vortex tube, even though the propagating disturbances may not form perfect independent wave modes.

Vortex tubes are ubiquitous in nature, particularly in turbulent flows (Rogers & Moin 1987; Sandham & Kleiser 1992; Vincent & Meneguzzi 1991, 1994; Cadot *et al.* 1995). These tubes are always subject to disturbances either due to their own axially varying structure (e.g. a simple core variation or a more complicated bending or unravelling) or to the influences of neighbouring vortices. Such a disturbance will create twist wave packets which propagate away along the tube. Such events have been observed experimentally (Hopfinger *et al.* 1982; Maxworthy *et al.* 1985) and in numerical simulations. In particular, in two companion papers (Andreassen *et al.* 1997; Fritts *et al.* 1997), we describe numerical simulations of a breaking gravity wave. After breaking, the gravity wave leaves a collection of vortex loops behind. Twist waves are not only common in the evolution of these vortex loops, but to a large degree dominate the evolution. These waves are large in amplitude (so large that they cause the ultimate demise of the tube), but their physics is identical to that discussed in the present paper for linearized waves. In particular, $m = 0$ waves are identified by the presence of an axisymmetric twist in the vorticity lines and accompanying regions of stretching/scrunching, as discussed in § 3. The scrunching is often so strong that it effectively breaks the tube apart by depleting its core of vorticity. Also, $m = 2$ waves are found that unravel single vortex tubes leaving two intertwined helices behind. The unravelling events propagate along a tube because of their own velocity fields and the vortex tilting that the velocity fields cause, as discussed in § 5.

It has been proposed that the evolution of vortex tube perturbations be interpreted using complex helical waves (Melander & Hussain 1995). Helical waves, which are not to be confused with Kelvin waves, are exact nonlinear solutions when taken individually, and may be superposed to represent any flow, except a potential flow (Lesieur 1987). Now, it is not only the vortex tube perturbation that is viewed as

https://doi.org/10.1017/S0022112097005958 Published online by Cambridge University Press

a sum of helical waves; the vortex tube *itself* is represented as a superposition of helical waves. Moreover, when present simultaneously, as they must be to represent a vortex tube, multiple helical waves couple nonlinearly; this coupling may dominate the dynamics (Melander & Hussain 1995) and hinder the interpretation of the results. Based on the results of the present paper, we suggest that the evolution of perturbations to a vortex tube be interpreted instead using twist waves. Twist waves appear to be the fundamental oscillation modes of a vortex tube, and they provide a straightforward physical understanding of the evolution of any initial perturbation. In the case of Kelvin waves for a straight tube of constant vorticity, these modes are complete so that any initial perturbation of the tube can be represented by a collection of twist waves.

Support for this work was provided by the Norwegian Defence Research Establishment, the National Science Foundation under grant ATM-9419151, and the Air Force Office of Scientific Research under grant F49620-95-1-0286. The authors wish to thank Thomas Bogdan for helpful discussions, and also an anonymous referee for useful comments.

Appendix A. Simplification of the initial condition functions

In this Appendix, we rewrite the initial condition functions $F(0)$ and $G(0)$ such that they are in terms of the initial vorticity distribution only. This is a particularly convenient way to specify an initial state of the vortex tube perturbation.

We begin with $F(0)$. First, the definition of the vorticity components ω_r and ω_z can be written as

$$\frac{\partial u_r}{\partial \phi} = \frac{\partial}{\partial r}(r u_\phi) - r\omega_z, \tag{A 1}$$

$$\frac{\partial u_\phi}{\partial z} = -\omega_r + \frac{1}{r}\frac{\partial u_z}{\partial \phi}. \tag{A 2}$$

Substituting these into the continuity equation, $\nabla \cdot \boldsymbol{u} = 0$, and simplifying, we obtain

$$\left[\frac{\partial^2}{\partial r^2} + \frac{1}{r}\frac{\partial}{\partial r} + \frac{1}{r^2}\frac{\partial^2}{\partial \phi^2} + \frac{\partial^2}{\partial z^2}\right]\frac{\partial u_z}{\partial \phi} = \frac{1}{r}\frac{\partial}{\partial r}\left(r\frac{\partial}{\partial r}(r\omega_r)\right) + \frac{\partial}{\partial z}\frac{1}{r}\frac{\partial}{\partial r}(r^2\omega_z) + \frac{1}{r}\frac{\partial^2 \omega_r}{\partial \phi^2}. \tag{A 3}$$

Using the divergence-free condition for the vorticity field, $\nabla \cdot \boldsymbol{\omega} = 0$, the right-hand side of this equation can be rewritten to be

$$\frac{\partial}{\partial \phi}\left[-\frac{1}{r}\frac{\partial}{\partial r}(r\omega_\phi) + \frac{1}{r}\frac{\partial \omega_r}{\partial \phi}\right], \tag{A 4}$$

so that

$$\left[\frac{\partial^2}{\partial r^2} + \frac{1}{r}\frac{\partial}{\partial r} + \frac{1}{r^2}\frac{\partial^2}{\partial \phi^2} + \frac{\partial^2}{\partial z^2}\right] u_z = \left[-\frac{1}{r}\frac{\partial}{\partial r}(r\omega_\phi) + \frac{1}{r}\frac{\partial \omega_r}{\partial \phi}\right]. \tag{A 5}$$

Fourier transforming and assuming ϕ-dependences of $\exp(im\phi)$ in (A 5), and using the result in (2.24), we find

$$F(0) = \frac{-1}{(s + im\Omega)^2}\left[-\frac{1}{r}\frac{\partial}{\partial r}\left(r\frac{\partial \omega_\phi}{\partial t}\right) + \frac{im}{r}\frac{\partial \omega_r}{\partial t}\right](0) - \frac{s + 2im\Omega}{(s + im\Omega)^2}\left[-\frac{1}{r}\frac{\partial}{\partial r}(r\omega_\phi) + \frac{im}{r}\omega_r\right](0). \tag{A 6}$$

https://doi.org/10.1017/S0022112097005958 Published online by Cambridge University Press

The time derivatives can be calculated with the aid of the vorticity equation, which is presented in Appendix C. Substituting $\partial\omega_r/\partial t$ and $\partial\omega_\phi/\partial t$ from (C 3) into (A 6), we find

$$F(0) = \frac{2\Omega \mathrm{i}k}{(s+\mathrm{i}m\Omega)^2}\omega_z(0) - \frac{1}{(s+\mathrm{i}m\Omega)}\left[\frac{1}{r}\frac{\partial}{\partial r}(r\omega_\phi) - \frac{\mathrm{i}m}{r}\omega_r\right](0). \tag{A 7}$$

We turn next to the expression for $G(0)$. Noting that

$$\omega_\phi = \frac{\partial u_r}{\partial z} - \frac{\partial u_z}{\partial r}, \tag{A 8}$$

we can rewrite $G(0)$ immediately as

$$G(0) = \frac{1}{\mathrm{i}k}\frac{4\Omega^2}{4\Omega^2+(s+\mathrm{i}m\Omega)^2}\left[-\frac{1}{4\Omega^2}\frac{\partial\omega_\phi}{\partial t} - \frac{s+2\mathrm{i}m\Omega}{4\Omega^2}\omega_\phi + \frac{\mathrm{i}m}{2\Omega r}u_z\right](0). \tag{A 9}$$

Using $\partial\omega_\phi/\partial t$ from the linearized vorticity equation (C 3), this becomes

$$G(0) = \frac{1}{\mathrm{i}k}\frac{4\Omega^2}{4\Omega^2+(s+\mathrm{i}m\Omega)^2}\left[\frac{\omega_r}{2\Omega} - \frac{s+\mathrm{i}m\Omega}{4\Omega^2}\omega_\phi\right](0). \tag{A 10}$$

Appendix B. Inversion of the Laplace transform

In this Appendix, we invert the Laplace transform to obtain $\tilde{u}_z^i$ and $\tilde{u}_z^o$ in the time domain. To do this, we will show that $\tilde{u}_z^i$ and $\tilde{u}_z^o$ as given in (2.29) and (2.32) respectively with A and B given in (2.35) and (2.36) are analytic functions of s except at simple poles given by the Kelvin wave mode eigenvalues and except at $s = -\mathrm{i}m\Omega$. The point at $s = -\mathrm{i}m\Omega$ will be shown to give no contribution to the integral, permitting us the considerable simplification of using Cauchy's theorem in the inversion of the Laplace transform.

The proof of analyticity is easier for $\tilde{u}_z^o$ than $\tilde{u}_z^i$, the difference being in the amount of algebra required. For convenience we derive the result explicitly for $\tilde{u}_z^o$ only; the proof for $\tilde{u}_z^i$ follows in a similar fashion and is not given. To begin, we first simplify the form of $\tilde{u}_z^o$ by substituting $g(r)$ given by (2.30) into (2.32) and (2.36) to obtain

$$\tilde{u}_z^o = -\frac{K_m(kr)}{K_m(ka)}\,\frac{\displaystyle\int^a F(0)\xi^m J_m(k\xi r')r'\mathrm{d}r' + \mathrm{i}ka\;\xi^2 G(0)\;\xi^m J_m(k\xi a)}{\displaystyle ka\xi^{m+1}J_m'(k\xi a) + \left[\frac{2\mathrm{i}m\Omega}{(s+\mathrm{i}m\Omega)} + (k\xi a)^2\frac{K_m'(ka)}{kaK_m(ka)}\right]\xi^m J_m(k\xi a)}\,. \tag{B 1}$$

This is a convenient form for investigating the analyticity with respect to s.

Now, $\tilde{u}_z^o$ has explicit dependence on s in the denominator of (B 1), but it also has s-dependence hidden in ξ, $F(0)$, and $G(0)$. Consider first the s-dependence of $F(0)$ and $G(0)$. From (A 7), $F(0)$ is analytic in s except for poles of first and second order at $s = -\mathrm{i}m\Omega$. Similarly, from (A 10) and (2.31), $\xi^2 G(0)$ is analytic in s except for poles of first and second order at $s = -\mathrm{i}m\Omega$.

Next, consider the s-dependence contained in ξ. Recall from (2.31) that

$$\xi^2 = -\frac{4\Omega^2}{(s+\mathrm{i}m\Omega)^2} - 1. \tag{B 2}$$

So, ξ^2 is an analytic function of s, except at $s = -\mathrm{i}m\Omega$, but ξ has a branch cut due to the square root. This branch cut will not affect our results, as we will show that $\tilde{u}_z^o$

https://doi.org/10.1017/S0022112097005958 Published online by Cambridge University Press

is actually a function of ξ^2 rather than ξ. To see this, use the series expansion for the Bessel function $J_m(k\xi a)$ to show

$$\xi^m J_m(k\xi a) = \left(\frac{ka}{2}\right)^m \xi^{2m} \sum_{j=0}^{\infty} \frac{1}{j!(m+j)!}\left(-\frac{k\xi a}{2}\right)^{2j}. \tag{B 3}$$

Since m is an integer in our case, this series is clearly a function of ξ^2. Moreover, it converges uniformly for all ξ^2 (except as $|\xi^2| \to \infty$). Therefore, $\xi^m J_m(k\xi a)$ is analytic in ξ^2; a similar result holds true for $\xi^{m+1} J'_m(k\xi a)$. Since a composite of analytic functions is analytic (see e.g. Marsden 1973), it follows that $\xi^m J_m(k\xi a)$ and $\xi^{m+1} J'_m(k\xi a)$ are analytic in s except at the point $s = -\mathrm{i}m\Omega$. At $s = -\mathrm{i}m\Omega$, the Bessel functions display an essential singularity.

Combining the results of the last two paragraphs, then, we find that the numerator and the denominator of $\tilde{u}_z^o$ given by (B 1) are both analytic functions of s except at $s = -\mathrm{i}m\Omega$. It follows that $\tilde{u}_z^o$ is analytic in s except at $s = -\mathrm{i}m\Omega$ and at poles given by the zeros of the denominator (or, equivalently, at the Kelvin wave mode eigenvalues given by (2.19)). Were it not for the non-analyticity at $s = -\mathrm{i}m\Omega$, we could immediately perform the inversion of the Laplace transform of $\tilde{u}_z^o$ using Cauchy's residue theorem. Now, the behaviour of $\tilde{u}_z^o$ at $s = -\mathrm{i}m\Omega$ is strange. Whereas the Bessel functions in $\tilde{u}_z^o$ have an essential singularity there, $\tilde{u}_z^o$ itself is finite (we will show this below). Since $\tilde{u}_z^o$ is non-analytic only at a single point (rather than over a branch cut) and since $\tilde{u}_z^o$ is finite at this point, we argue that the contribution of this point to the Laplace transform inversion is zero.† Cauchy's theorem can then be applied, and the inverted $\tilde{u}_z^o$ is simply the sum of the residues at the Kelvin wave mode frequencies. For the examples given in § 3–5, we have checked this result by showing that the solution reproduces the correct initial conditions.

It remains to show that $\tilde{u}_z^o$ is finite at $s = -\mathrm{i}m\Omega$. Since $s = -\mathrm{i}m\Omega$ corresponds to $|\xi| \to \infty$, we use the asymptotic expansions for the Bessel functions to simplify (B 1). To proceed, we rewrite (B 1) as

$$u_z^o = -\frac{K_m(kr)}{K_m(ka)} \frac{\dfrac{aF(0)|_{r=a}}{J_m(k\xi a)} \displaystyle\int^a J_m(k\xi r')\mathrm{d}r' + \mathrm{i}ka\xi^2 G(0)}{\dfrac{k\xi a J_{m+1}(k\xi a)}{J_m(k\xi a)} + m + \dfrac{2\mathrm{i}m\Omega}{(s+\mathrm{i}m\Omega)} + (k\xi a)^2 \dfrac{K'_m(ka)}{kaK_m(ka)}}, \tag{B 4}$$

where the integral in the numerator has been replaced with the first term in its asymptotic expansion. The asymptotic expansion for Bessel functions of the first kind is

$$J_m(k\xi a) \sim \left(\frac{2}{\pi k\xi a}\right)^{1/2} \cos\left(k\xi a - \frac{m\pi}{2} - \frac{\pi}{4}\right). \tag{B 5}$$

Using this in (B 4), we find

$$u_z^o = -\frac{K_m(kr)}{K'_m(ka)} \left(\mathrm{i}G(0) + \frac{2aF(0)}{k\xi^2}\right) \tag{B 6}$$

to leading order in ξ^{-1}. Using (A 7) and (A 10) for $F(0)$ and $G(0)$ respectively and

† This argument is complicated by the fact that the point $s = -\mathrm{i}m\Omega$ is the accumulation point of the Kelvin wave mode frequencies.

https://doi.org/10.1017/S0022112097005958 Published online by Cambridge University Press

setting $s = -im\Omega$, we find

$$u_z^o = -\frac{1}{2k\Omega}\,\frac{K_m(kr)}{K_m'(ka)}\;(\omega_r(0) - 2ika\omega_z(0)). \tag{B 7}$$

Thus, u_z^o is finite at $s = -im\Omega$.

Appendix C. Linearized vorticity equation

The vorticity equation

$$\frac{\partial \boldsymbol{\omega}}{\partial t} = \nabla \times (\boldsymbol{u} \times \boldsymbol{\omega}) \tag{C 1}$$

can be linearized to be

$$\frac{\partial \boldsymbol{\omega}}{\partial t} = \hat{\boldsymbol{r}}\Omega\left(2\omega_\phi - \frac{\partial \omega_r}{\partial \phi} + 2\frac{\partial u_z}{\partial r}\right) + \hat{\boldsymbol{\phi}}\Omega\left(\frac{2}{r}\frac{\partial u_z}{\partial \phi} - 2\omega_r - \frac{\partial \omega_\phi}{\partial \phi}\right) + \hat{\boldsymbol{z}}\Omega\left(-\frac{\partial \omega_z}{\partial \phi} + 2\frac{\partial u_z}{\partial z}\right). \tag{C 2}$$

Using the fact that $\boldsymbol{\omega} = \nabla \times \boldsymbol{u}$, (C 2) can be rewritten in the convenient form

$$\mathrm{D}\boldsymbol{\omega} = 2\Omega\frac{\partial \boldsymbol{u}}{\partial z}, \tag{C 3}$$

where D has been defined in (2.8)

REFERENCES

Abramowitz, M. & Stegun, I. A. 1964 *Handbook of Mathematical Functions*. Dover.

Andreassen, Ø., Hvidten, P. Ø., Fritts, D. C. & Arendt, S. 1997 Vorticity dynamics in a breaking gravity wave 1: Initial instability evolution. *J. Fluid Mech.*, submitted.

Batchelor, G. K. 1967 *An Introduction to Fluid Dynamics*. Cambridge University Press.

Briggs, R. J., Daugherty, J. D. & Levy, R. H. 1970 Role of Landau damping in cross-field electron beams and inviscid shear flow. *Phys. Fluids* **13**, 421–432.

Cadot, O., Douady, S. & Couder, Y. 1995 Characterization of the low-pressure filaments in a three-dimensional turbulent shear flow. *Phys. Fluids* A **7**, 630–646.

Case, K. M. 1960 Stability of inviscid plane Couette flow. *Phys. Fluids* **3**, 143–148.

Crow, S. C. 1971 Stability theory for a pair of trailing vortices. *AIAA J.* **8**, 2172–2179.

Fritts, D. C., Arendt, S. & Andreassen, Ø. 1997 Vorticity dynamics in a breaking gravity wave 2: Vortex interactions and transition to turbulence. *J. Fluid Mech.* submitted.

Hasimoto, H. 1972 A soliton on a vortex filament. *J. Fluid Mech.* **51**, 477–485.

Hopfinger, E. J., Browand, F. K. & Gagne, Y. 1982 Turbulence and waves in a rotating tank. *J. Fluid Mech.* **125**, 505–534.

Kelvin, Lord 1880 Vibrations of a columnar vortex. *Phil. Mag.* **10**, 155–168.

Lamb, H. 1945 *Hydrodynamics*. Dover.

Leibovich, S., Brown, S. N. & Patel, Y. 1986 Bending waves on inviscid columnar vortices. *J. Fluid Mech.* **173**, 595–624.

Leibovich, S. & Ma, H. Y. 1983 Soliton propagation on vortex cores and the Hasimoto soliton. *Phys. Fluids* **26**, 3173–3179.

Lesieur, M. 1987 *Turbulence in Fluids*. Martinus Nijhoff.

Lessen, M., Singh, P. J. & Paillet, F. 1974 The stability of a trailing line vortex. Part 1. Inviscid theory. *J. Fluid Mech.* **63**, 753–763.

Marsden, J. E. 1973 *Basic Complex Analysis*. Freeman.

Maxworthy, T., Hopfinger, E. J. & Redekopp, L. G. 1985 Wave motions on vortex cores. *J. Fluid Mech.* **151**, 141–165.

Mayer, E. W. & Powell, K. G. 1992 Viscous and inviscid instabilities of a trailing vortex. *J. Fluid Mech.* **245**, 91–114.

https://doi.org/10.1017/S0022112097005958 Published online by Cambridge University Press

Melander, M. V. & Hussain, F. 1993 Coupling between a coherent structure and fine-scale turbulence. *Phys. Rev.* E **48**, 2669–2689.

Melander, M. V. & Hussain, F. 1994 Core dynamics on a vortex column. *Fluid Dyn. Res.* **13**, 1–37.

Melander, M. V. & Hussain, F. 1995 Polarized vorticity dynamics on a vortex column. *Phys. Fluids* A **5**, 1992–2003.

Moore, D. W. & Saffman, P. G. 1972 The motion of a vortex filament with axial flow. *Phil. Trans. R. Soc. Lond.* A **272**, 403–429.

Moore, D. W. & Saffman, P. G. 1975 The instability of a straight vortex filament in a strain field. *Proc. R. Soc. Lond.* A **346**, 413–425.

Rogers, M. M. & Moin, P. 1987 The structure of the vorticity field in homogeneous turbulent flows. *J. Fluid Mech.* **176**, 33–66.

Saffman, P. G. 1992 *Vortex Dynamics*. Cambridge University Press.

Sandham, N. D. & Kleiser, L. 1992 The late stages of transition to turbulence in channel flow. *J. Fluid Mech.* **245**, 319–348.

Schoppa, W., Hussain, F. & Metcalfe, R. W. 1995 A new mechanism of small scale transition in a plane mixing layer: core dynamics of spanwise vortices. *J. Fluid Mech.* **298**, 23–80.

Tsai, C.-Y. & Widnall, S. E. 1976 The stability of short waves on a straight vortex filament in a weak externally imposed strain field. *J. Fluid Mech.* **73**, 721–733.

Verzicco, R., Jiménez, J. & Orlandi, P. 1995 On steady columnar vortices under local compression. *J. Fluid Mech.* **299**, 367–388.

Vincent, A. & Meneguzzi, M. 1991 The spatial structure and statistical properties of homogeneous turbulence. *J. Fluid Mech.* **225**, 1–20.

Vincent, A. & Meneguzzi, M. 1994 The dynamics of vorticity tubes in homogeneous turbulence. *J. Fluid Mech.* **258**, 245–254.

https://doi.org/10.1017/S0022112097005958 Published online by Cambridge University Press